# Tensile and Flexure Strength of Unidirectional Fiber-Reinforced Composites: Direct Numerical Simulations and Analytic Models

Glenn C. Foster

Thesis submitted to the Faculty of the
Virginia Polytechnic Institute and State University
in partial fulfillment of the requirements for the degree of

Master of Science
in
Engineering Mechanics

William A. Curtin, Jr., Chair
Edmund G. Henneke, II
Romesh C. Batra

February 20, 1998
Blacksburg, Virginia

Keywords: fiber reinforced composite, load sharing, metal matrix composite, modeling, simulation, flexure strength, ultimate tensile strength

©1998 Glenn C. Foster

# Tensile and Flexure Strength of Fiber-Reinforced Composites: Direct Numerical Simulations and Analytic Models

Glenn C. Foster
Department of Engineering Science and Mechanics
Virginia Polytechnic Institute and State University
Blacksburg, VA 24061-0219

**Abstract**

A Local Load Sharing (LLS) model recently developed by Curtin and co-workers for the numerical simulation of tensile stress-strain behavior in fiber-reinforced composites is used to predict the tensile strength of metal matrix composites consisting of a Titanium matrix and unidirectionally aligned SiC fibers. This model is extended to include the effects of free boundary conditions and non-constant load gradients and then used to predict the strength of a Ti-6Al-4V matrix reinforced with Sigma SiC fibers under 4-point flexure testing. The predicted tensile and flexure strengths agree very well with the values measured by Gundel and Wawner and Ramamurty et al. The composite strength of disordered spatial fiber distributions is investigated and is shown to have a distribution similar to the corresponding ordered composite, but with a mean strength that decreases (as compared to the ordered composite) with increasing Weibull modulus. A modified Batdorf-type analytic model is developed and similarly extended to the case of non-uniform loading to predict the strength of composites under tension and flexure. The flexure model is found to be inappropriate for application to the experimental materials, but the tensile model yields predictions similar to the Local Load Sharing models for the experimental materials. The ideas and predictions of the Batdorf-type model, which is essentially an approximation to the simulation model, are then compared in more detail to a simulation-based model developed by Ibnabdeljalil and Curtin to more generally assess the accuracy of the Batdorf model in predicting tensile strength and notch strength versus composite size and fiber Weibull modulus. The study shows the Batdorf model to be accurate for tensile strength at high Weibull moduli and to capture general trends well, but it is not quantitatively accurate over the full range of material parameters encountered in various fiber composite systems.

# Acknowledgments

The author would like to thank the following people for their contributions and support of this work:

- First and foremost, Dr. William A. Curtin, Jr., my advisor and mentor, a man of almost limitless patience, the depths of which may never have been fully probed if he hadn't taken me on as his student.

- Dr. Edmund Henneke and Dr. Romesh Batra, for making time in their busy schedules to serve on my committee.

- The National Science Foundation and the Air Force Office of Scientific Research for their financial support of this work.

- Cindy Hopkins, Nancy Linkous, Sheila Collins, Loretta Trickle, and everyone else who navigated me through the paperwork and processes of graduate school.

- My fellow denizens of Femoyer Hall (past and present): Jian, Yanhua, Senthil, Rakesh, Hung-Peng, Myung-Hyun, Clifton, Isam, Sanjiv, Andy, and Reza for their friendship and advice.

- Kareema McLendon, I can not imagine a more wonderful distraction from any problem in this world. My everlasting gratitude and love are yours.

- My parents and family, thank you for your support and understanding; I promise I will go out and get a real job soon.

# Contents

**Acknowledgments** **iv**

**List of Figures** **ix**

**List of Tables** **x**

**1 Introduction and Background** **1**
1.1 Introduction . . . 1
1.2 Composite Mechanics . . . 3
1.2.1 Elastic properties . . . 3
1.2.2 Variability of Fiber Strength . . . 4
1.2.3 Matrix Failure . . . 5
1.2.4 Fiber Debonding and Slip . . . 5
1.2.5 Normalized Characteristic Length and Strength . . . 6
1.2.6 Load Transfer and Fiber Bundle Failure . . . 7
1.3 Outline . . . 7

**2 Models of Composite Tensile Strength** **9**
2.1 Common Ground . . . 9
2.2 Global Load Sharing (GLS) . . . 10
2.3 Numerical Local Load Sharing (LLS) . . . 10
2.4 Analytic Local Load Sharing (LLS) . . . 12
2.5 Modified Batdorf . . . 13
2.6 Comparison of Modified Batdorf and LLS models . . . 17
2.6.1 Size Scaling . . . 18
2.6.2 Notch Strength . . . 20
2.7 Summary . . . 23

**3 Boundary Effects and Heterogeneous Loads** **25**
3.1 Motivation . . . 25
3.2 Modeling Procedure and Boundary Effects . . . 26
3.3 Results: Periodic vs. Free Boundary . . . 28
3.4 Random Fiber Arrangements . . . 31
3.5 Results: Checkerboard vs. Random . . . 34
3.6 Load Gradients: Flexure Testing . . . 41
3.7 Modeling Flexure Load Gradients . . . 41
3.8 A Modified Batdorf Model for Flexure . . . 43
3.9 Summary . . . 45

**4 Comparison to Experiment** **47**
4.1 Tension . . . 47
4.1.1 Ti-1100/SCS-6 . . . 47
4.1.2 Ti-6Al-4V/BP-Sigma . . . 51
4.2 Summary of Tensile Results . . . 52
4.3 Flexure . . . 53

**5 Summary, Conclusions, and Future Work** **57**

**Bibliography** **59**

**Notation** **62**

**Vitæ** **64**

# List of Figures


1.1 Unidirectional fiber-reinforced composite. . . . . 3
1.2 Stress-Strain curve of an idealized fiber-reinforced composite. . . . . 4
1.3 Deformation and stress distribution around fiber breaks . . . . . 6

2.1 Partitioning of the simulated composite . . . . . 11
2.2 Evolution of failure in the Batdorf model. . . . . 16
2.3 Fiber bundle strength versus composite volume for the Batdorf and LLS models at m=2,5. . . . . 19
2.4 Fiber bundle strength versus composite volume for the Batdorf and LLS models at m=10 . . . . . 20
2.5 Fiber bundle strength vs initial notch size. . . . . 22

3.1 Example of stress redistribution due to a break away from a boundary. 27
3.2 Stress redistribution due to a break at a free boundary. . . . . 28
3.3 Stress redistribution due to a break at the corner of free boundaries. . 29
3.4 Semi-free boundary cross section. . . . . 30
3.5 Free boundary cross section. . . . . 30
3.6 Example of stress redistribution due to a break in a random lattice with a locally high concentration of fibers. . . . . 32
3.7 Example of stress redistribution due to a break in a random lattice with a lower concentration of fibers in the immediate vicinity of the break. . . . . 33
3.8 Example of stress redistribution due to a break in a checkerboard lattice 34
3.9 Cumulative failure probability distribution versus stress of random and checkerboard lattices at $m = 5$ and 10. . . . . 37
3.10 Failure planes of ordered and disorded lattices for $m$=5. . . . . 38
3.11 Failure planes of ordered and disorded lattices for $m$=10. . . . . 39
3.12 Predicted scaling of strength with increasing composite size. . . . . 40
3.13 Plane stress flexure (3-pt bend) . . . . . 42
3.14 Beam under 4-point bend . . . . . 43

4.1 Experimental and predicted ultimate tensile strengths . . . . . 50

4.2 Fiber bundle flexure stress vs. cumulative fiber breaks . . . . . 55
4.3 Evolution of simulated composite failure under 4-point flexure. . . . . 56

# List of Tables

2.1 Global Load Sharing results for various intrinsic link sizes. . . . . 14
2.2 Stress concentration factors and number of near neighbors for various failure cluster sizes. . . . . 17

3.1 Fiber-bundle strengths of simulated composites having free, semi-free, and periodic boundary conditions . . . . . 31
3.2 Fiber-bundle strengths of random and regular lattices. . . . . 36

4.1 Measured constitutive properties of MMC samples . . . . . 48
4.2 Composite tensile strengths of MMCs . . . . . 49
4.3 Fiber bundle strength estimates and predictions for the Ti-6Al-4V MMC under 4-point bending. . . . . 53

# Chapter 1

# Introduction and Background

*I have yet to see any problem, however complicated, which, when you looked at it the right way, did not become still more complicated.*

—Paul Anderson, *New Scientist*

*You can see a lot just by looking.*

— Yogi Berra

## 1.1 Introduction

Composite structures combine materials which together result in a structure with properties not achievable with any of the constituents alone. Fiber-reinforced composites, specifically those based on ceramic and metal matrix materials, combine the best of both materials; inheriting the high stiffness and strength from the fibers while preserving the elevated temperature capabilities of the matrix material. In addition, the fiber-reinforced material tends to be more resistant to damage and defects than the homogeneous material. Cracks in the matrix are either shortened by an encounter with a fiber or occur parallel to the fiber, which, presumably is in the loading direction, causing little effect on the tensile strength. The matrix keeps the fibers together and oriented, protects the fibers from the environment (e.g. moisture, surface abrasion) and each other (fibers rubbing against each other), and acts as a load-transfer medium between fibers. For uniaxial fiber-reinforced composites (all fibers are oriented in the same direction), the ability to bear a tensile load is greatest in the direction of fiber orientation, and consequently the tensile strength in this direction is a key parameter when designing engineered materials of this type.

The fracture mechanics of conventional brittle material failure is governed by crack growth from pre-existing damage. In contrast, failure of ceramic matrix com-

posites (CMC's), metal matrix composites (MMC's), and polymer matrix composites (PMC's) occurs due to the accumulation and interaction of individual fiber breaks which develop as the material is loaded until a "critical" amount of damage is formed, precipitating failure.

Various models of fiber damage accumulation have been developed. In this study, models under examination will be based on the ideas of Global Load Sharing (GLS) and Local Load Sharing (LLS). The difference between the two models is in the way broken fibers transfer their load to other fibers in the composite. Under GLS, broken fibers transfer their load to all intact fibers in the cross-section of the break equally, while a LLS rule transfers the bulk of the load to fibers in a neighborhood around the break.

Models based on GLS have had fair success in predicting the tensile strength (Curtin, 1991; MacKay et al., 1991; Weber et al., 1996) but are also popular due to their ease of use and relatively simple closed form expressions for the ultimate strength. These models incorporate considerable micromechanical and material properties (in-situ fiber strength, fiber diameter, residual stresses, interfacial sliding resistance, and matrix yield stress), and have been extended to include matrix creep and time-dependent fiber degradation to predict deformation and damage accumulation (Fabeny and Curtin, 1996; Du and McMeeking, 1995; Iyengar and Curtin, 1997).

Much of the recent work on LLS models (Zhou and Curtin, 1995; Ibnabdeljalil and Curtin, 1998; Cox et al., 1994; Xu et al., 1995) have come about in an attempt to overcome some of the shortcomings in the GLS model. Some of the things that can be "fixed" by including local stress concentrations include:

- Lower strength predictions (GLS overpredicts, and actually provides an upper limit on strength.)
- Size dependent strength ( Strength should depend on composite volume)
- Material reliability and failure probability predictions are possible
- Effects of notches, local concentrated damage, and geometry effects

Especially important is the effect of size on strength, so that differences in strength between test coupons and large "real world" components can be studied. Unfortunately these gains result in the loss of GLS's simple analytic formulation; the extreme increase in complexity of damage and failure processes under LLS necessitate numerical simulation techniques.

**Figure 1.1** Unidirectional fiber-reinforced composite.

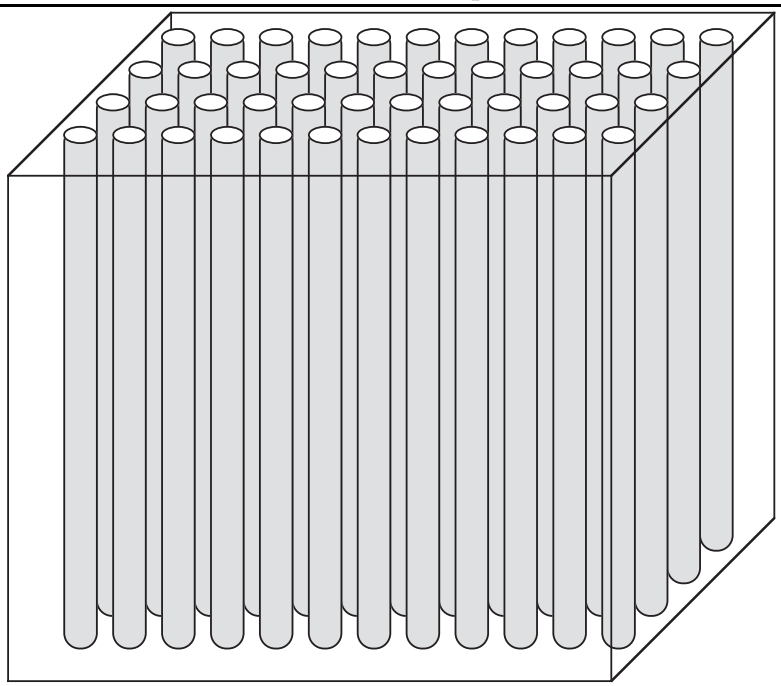

## 1.2 Composite Mechanics

### 1.2.1 Elastic properties

Consider a unidirectional composite, as depicted in Figure 1.1. When subjected to a load in the longitudinal direction, the strain $\epsilon$ in the matrix will be the same as the strain in the fiber as long as the fiber is perfectly bonded to the matrix. Assuming the matrix and fibers both behave linear-elastically, the axial stresses in the fibers and matrix are approximated by:

$$\sigma_f = E_f\epsilon \quad , \quad \sigma_m = E_m\epsilon \tag{1.1}$$

where $E_f$, $E_m$ are the Young's moduli of the fibers and matrix respectively. To achieve any advantage by fiber reinforcement, $E_f$ should be larger than $E_m$, so the fiber stress is higher than that of the matrix. A load $P$ applied to the composite is therefore split between the materials as

$$P = \sigma_f A_f + \sigma_m A_m \tag{1.2}$$

where $A_f$ and $A_m$ are the cross-sectional areas of the fibers and matrix respectively. If the cross-section of the specimen has area $A$, then we define the volume fraction of

**Figure 1.2** Stress-Strain curve of an idealized fiber-reinforced composite. Region I corresponds to an elastic matrix. Region II corresponds to a plastically yielding matrix. Fibers are assumed to behave elastically up to failure.

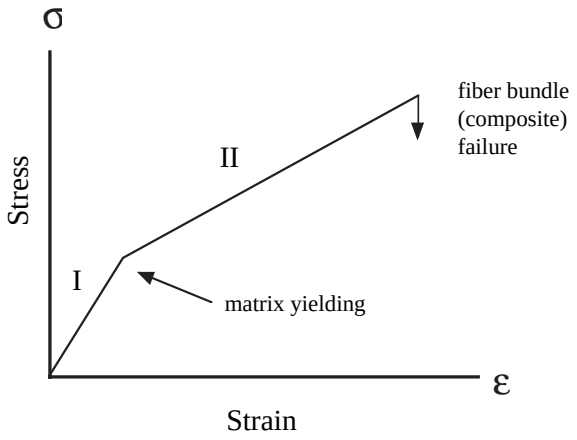


the fibers by $f = \frac{A_f}{A}$. Since the volume fraction for the matrix would be $1 - f = \frac{A_m}{A}$ we get the *Rule of Mixtures* equation:

$$\langle \sigma \rangle = f\langle \sigma_f \rangle + (1 - f)\langle \sigma_m \rangle \tag{1.3}$$

where $\langle \sigma_f \rangle$ is the average stress in the fibers and $\langle \sigma_m \rangle$ is the average stress in the matrix, valid in the stress-strain regime where both fiber and matrix behave linear-elastically. This regime corresponds to region I of the stress-strain curve illustrated in Figure 1.2.

### 1.2.2 Variability of Fiber Strength

Fibers tend to be brittle solids and, due to flaws along their lengths, their strengths are statistical in nature. Fibers (and other brittle solids) are customarily described using a Weibull distribution (Weibull, 1939; Weibull, 1951). The cumulative probability of fiber failure $P_f(\sigma, L)$ in a length $L$ at an applied tensile stress $\sigma$ can be expressed using a two-parameter Weibull distribution:

$$P_f(\sigma, L) = 1 - e^{-\frac{L}{L_o}\left(\frac{\sigma}{\sigma_o}\right)^m} \tag{1.4}$$

where $\sigma_o$ is the characteristic fiber strength at gauge length $L_o$ and $m$ is the "Weibull modulus" describing the variation in fiber strengths (a high $m$ indicates a low vari-

ability in strength). The mean strength of a *single* fiber of length $L$ is then

$$\langle \sigma_{sf} \rangle = \int_0^\infty \sigma \, \frac{dP_f}{d\sigma} \, d\sigma = \sigma_o \left( \frac{L_o}{L} \right)^{\frac{1}{m}} \Gamma \left( 1 + \frac{1}{m} \right) \tag{1.5}$$

where $\Gamma(\bullet)$ is the usual Gamma function. So, for example, if the length of a fiber examined is increased by a factor of 10, then an $m$ of 10 results in a 21% decrease in mean strength while an $m$ of 3 results in a 54% decrease in mean strength when compared to the original fiber length.

### 1.2.3 Matrix Failure

In a metal matrix composite under an applied tensile load, the first non-linear event is matrix yielding. Beyond this yield stress the matrix is assumed to be perfectly plastic; the fibers must carry the remaining load so that

$$\sigma = f\sigma_f + (1 - f)\sigma_y \tag{1.6}$$

where $\sigma_f$ is the load carried by the fiber bundle and $\sigma_y$ is the matrix yield stress. This is shown as region II in Figure 1.2.

### 1.2.4 Fiber Debonding and Slip

We have assumed that as the applied tensile load was increased up to the point of matrix failure that few to none of the fibers have broken. As the load is increased, individual breaks will form at the weaker flaws along the fibers. At the point of fiber failure, the fiber/matrix interface debonds, with the fiber sliding against the matrix with interfacial sliding resistance $\tau$. For simplicity and tractability we at this time assume $\tau$ to be constant. Balancing the shear load to the tensile load we find the tensile load on the fiber will increase with distance from the break according to

$$\pi r^2 \, d\sigma = 2\pi r \tau \, dy \tag{1.7}$$

which simplifies to

$$\frac{d\sigma}{dy} = \frac{2\tau}{r} \tag{1.8}$$

where the fiber radius is $r$. So the stress in the fiber at a break is zero, and attempts to recover linearly to the far-field load $\sigma_f$ over a slip length $l_s = r\sigma_f / 2\tau$, as illustrated in Figure 1.3.

**Figure 1.3** (a) Deformation around a single fiber composite element with multiple breaks undergoing a tensile load parallel to the fiber. (b) Corresponding tensile stress distribution along the fiber.

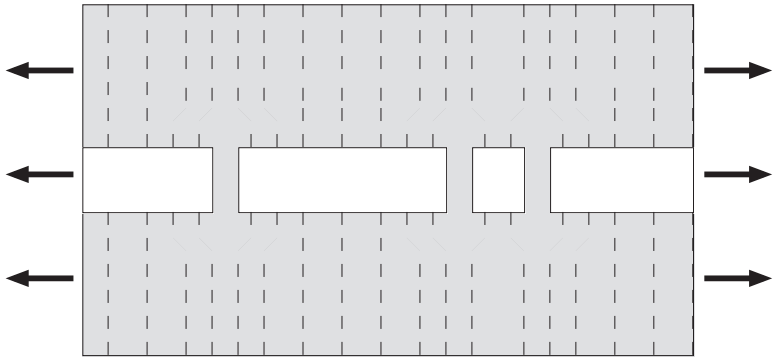

(a)

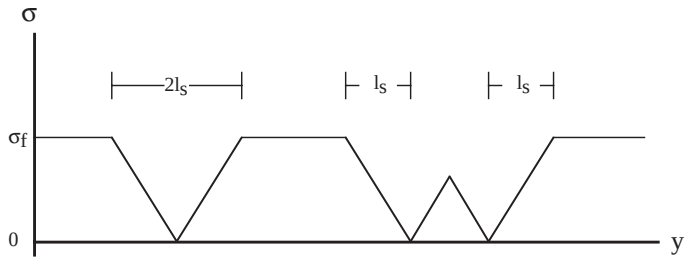


(b)

### 1.2.5 Normalized Characteristic Length and Strength

The reference stress $\sigma_o$ in Equation 1.4 is the characteristic ($1-e^{-1} \simeq 0.632$) strength of a fiber of length $L_o$ in a tension test. The average number of defects that can fail at stress $\sigma$ in a length $L$ is given by

$$N(\sigma, L) = \frac{L}{L_o}\left(\frac{\sigma}{\sigma_o}\right)^m \tag{1.9}$$

so it can be seen that $\sigma_o$ is the stress needed, on average, to cause one failure in a fiber of length $L_o$.

If we consider a single fiber embedded in a matrix, a natural characteristic length and characteristic strength arise from these strength statistics and our assumptions about slip. We define $\delta_c$ as the sliding length (twice the slip length) of a fiber fragment at a characteristic strength $\sigma_c$, so

$$\delta_c = 2l_s = r\sigma_c/\tau \tag{1.10}$$

However if we require $\sigma_c$ to be the average strength of a fiber of length $\delta_c$, then this implies

$$N(\sigma_c, \delta_c) = 1 = \frac{\delta_c}{L_o}\left(\frac{\sigma_c}{\sigma_o}\right)^m \tag{1.11}$$

Combining these two equations, we get

$$\sigma_c = \left(\frac{\sigma_o^m \tau L_o}{r}\right)^{\frac{1}{m+1}} \qquad \delta_c = \left(\frac{\sigma_o r L_o^{\frac{1}{m}}}{\tau}\right)^{\frac{m}{m+1}} \quad . \tag{1.12}$$

In general, most stresses and lengths in the rest of this work will be normalized by these quantities; we often refer to them as the "critical" stress and length. We will find that the composite strength is proportional to $\sigma_c$ and that the pullout distribution in the fracture surface is proportional to $\delta_c$.

### 1.2.6 Load Transfer and Fiber Bundle Failure

Load that was previously carried by the slipping section of a broken fiber is transferred to unbroken fibers in the neighborhood of the break, increasing the load on the intact fibers. As loading increases and damage accumulates, clusters of breaks form, growing larger as they transfer increasing amounts of stress to vulnerable intact fibers nearby. At some point, a critical stress $\sigma_f^*$ is reached, where one cluster grows continuously until the entire composite fails. The composite ultimate tensile strength (UTS) is then

$$\sigma_u = f\sigma_f^* + (1-f)\sigma_y \quad . \tag{1.13}$$

All analytic and numerical models in this work will focus on calculating $\sigma_f^*$ and use Equation 1.13 when comparing to experimental results.

## 1.3 Outline

In this chapter we have established some of the background and assumptions that we will use in later models of composite strength.

In Chapter 2 we will review some well established models such as the Global Load Sharing model (Curtin, 1991). We will also examine a more recent numerically based Local Load Sharing model (Zhou and Curtin, 1995) and an analytic model (Ibnabdeljalil and Curtin, 1998) derived from the results of this model. We will form an analytic model based on the concepts developed by Batdorf (1982) which includes some but not all of the features of the Local Load Sharing simulation model. To investigate the more general utility of the Batdorf model, we then perform a detailed comparisons of the predicted scaling of strength with composite volume and of the

notch strength versus notch size between the Batdorf model and the analytic Local Load Sharing model.

In Chapter 3 we extend the Local Load Sharing simulation model to include the effects of free boundaries and examine the changes in local stress redistribution as well as effects on the overall strength of the composite. The effects of spatially distributed fibers (as opposed to an ordered lattice) on the on the local stress redistribution and total composite strength are examined as well. Applying the results of these simulations to the analytic Local Load Sharing model, we make predictions of the strength of similar systems whose size is considerably larger.

The free-boundary Local Load Sharing model is further extended to include non-constant load gradients, specifically the load gradients of beams subjected to flexure. The Batdorf model is similarly extended (for thick composites) to predict the strength of composites undergoing flexure testing.

In Chapter 4 we apply these models using the physical properties of real composites and compare the predictions to the experimental results. Tensile tests performed by Gundel and Wawner (1997) on a composite consisting of Ti-1100 matrix material reinforced with SCS-6 SiC fibers are compared to the predictions made by the various models discussed in Chapter 2. Similarly, tests performed on a Ti-6Al-4V alloy reinforced with Sigma SiC fibers by Ramamurty et al. (1998) are also compared to model predictions, but these tests include flexure as well as tensile results.

Conclusions and some possible directions for future work are discussed in Chapter 5.

# Chapter 2

# Models of Composite Tensile Strength

*It is a test of true theories not only to account for but to predict phenomena.*

—William Whewell, *Philosophy of the Inductive Sciences*

*It's tough to make predictions, especially about the future.*

—Yogi Berra

In this chapter we will discuss in more detail the models that were mentioned earlier: the Global Load Sharing (GLS) model and a few inter-related Local Load Sharing (LLS) models. We will compare the effects of size-scaling (increasing the size of the composite) and notching (intentionally damaging the composite) on the predicted strengths in some of these LLS models

## 2.1 Common Ground

The models under discussion all simulate the same idealized composite: a square array of $n$ parallel fibers of radius $r$, Young's modulus $E_f$, embedded in a matrix. The matrix is assumed to have reached its matrix damage state, i.e., plastically yielded in the case of metal matrix composites, multiply cracked in the case of ceramic matrix composites, or simply possesing very low strength in the case of polymer matrix composites. A further assumption is that the fiber/matrix interface is relatively weak resulting in a debonded sliding interface controlling the interface shear stress $\tau$ either during matrix cracking, fiber fracture, or shear yielding by the matrix. For simplicity, $\tau$ is assumed to be constant in a sliding/yielding region,

resulting in a stress distribution around a break that recovers linearly with distance, from zero at the break to the far-field fiber stress $\sigma$ at a distance

$$l_s = r\sigma/2\tau \qquad . \tag{2.1}$$

## 2.2 Global Load Sharing (GLS)

Under Global Load Sharing, where there are no local stress concentrations, it has been shown that a characteristic fiber strength $\sigma_c$ and gauge length $\delta_c$ arise (Curtin, 1991). While these quantities were discussed previously in Section 1.2.5, Equation 1.12 merits being mentioned again. Those characteristic quantities are given by

$$\sigma_c = \left(\frac{\sigma_o^m \tau L_o}{r}\right)^{\frac{1}{m+1}} \qquad \delta_c = \left(\frac{\sigma_o r L_o^{\frac{1}{m}}}{\tau}\right)^{\frac{m}{m+1}} \qquad . \tag{2.2}$$

Physically, $\sigma_c$ is the characteristic fiber strength at a length $\delta_c$ while $\delta_c$ is, in turn, twice the slip length at an applied stress of $\sigma_c$. The critical fiber bundle stress $\sigma_f^*$ is directly proportional to $\sigma_c$, and the distribution of fiber lengths protruding from the fracture surface (fiber "pullout") is directly proportional to $\delta_c$. For the Weibull moduli arising in the present work ($m \geq 5$), a simple but accurate analytic result for the UTS has been given by Curtin and Zhou (1995):

$$\sigma_u = f\sigma_c \left(\frac{m}{2}\right)^{\frac{m}{m+1}} \left[1 - e^{(-2/m)}\right] + (1-f)\sigma_y \qquad . \tag{2.3}$$

An exact result for the GLS problem has been developed recently by Phoenix et al. (1997), which is not, however, compactly described.

## 2.3 Numerical Local Load Sharing (LLS)

*Its failures were the result of bad local agents*
—W. E. B. Du Bois, *The Souls of Black Folk*

To follow the evolution of fiber damage under LLS, where broken fibers transfer stress only to nearby unbroken fibers, Zhou and Curtin (1995) and Ibnabdeljalil and Curtin (1998) have developed a numerical simulation model.

The composite is partitioned into a regular array of $N_x \times N_y \times N_z$ fiber elements as shown in Figure 2.1. If the longitudinal direction of the fibers is chosen to be the $y$-axis, then we discretize the system so that the composite is of length $N_y\bar{\delta}$ and

**Figure 2.1** Partitioning of the simulated composite showing length scales.

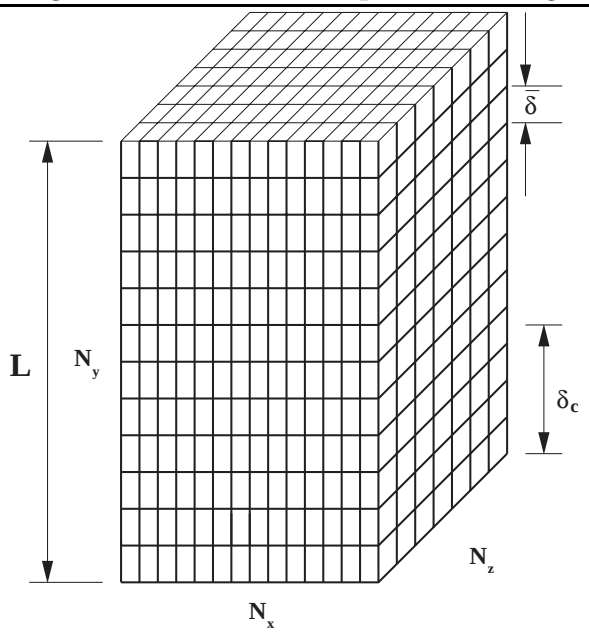


consists of an array of $N_x \times N_z$ fibers. We pick $\bar{\delta}$ to be much smaller than $\delta_c$ since that is the length scale where all the interesting behavior occurs

The model represents each fiber as a string of individual springs, and the fibers are coupled to each other through orthogonal shear springs which serve to transfer load when a fiber breaks. The statistical distribution of fiber strengths is introduced as the strength distribution of the individual springs: each fiber element is assigned a random strength from the appropriate Weibull distribution. Fiber slippage along a fiber after breaking is directly included by using our usual linear slip rule (Equation 2.1).

An important assumption is made that the tensile load bearing capacity of the matrix is ignored at this stage, which is reasonable *when fiber failure controls composite failure.*

The load transfer occurs naturally due to the shear springs; the ratio of shear modulus $k_s$ to tensile modulus $k_t$, $\Omega^2 = k_s/k_t$, is an adjustable parameter in the model. Changing $\Omega$ changes the load sharing as follows: $\Omega \to \infty$ corresponds to GLS, while $\Omega \to 0$ corresponds to extreme LLS. For this work we will use $\Omega = 0.001$ and arrange the fibers in a regular square array. The resulting load transfer is identical to that derived by Hedgepeth and van Dyke (1967) in their classic work, such that a single broken fiber transfers 14.5% of its load to its four near neighbors, 6% to its four corner neighbors, and lesser amounts to more distant neighbors.

The Green's function technique of Zhou and Curtin (1995) is used to efficiently accomplish the numerically-demanding process of transferring all of the stress in a manner that is consistent with the spatially-distributed array of fiber breaks that arises during loading of the composite. A Green's function is essentially a response function $G_{ij}$ which (in this case) relates the displacement of a point $i$ in a lattice due to the application of a force at a point $j$. When fibers are broken or slipping (broken or plastic springs), a new Green's function can be calculated, in part by inverting the original $G_{ij}$. The new Green's function now describes the stress distribution around broken and slipping fibers at various locations. Clusters of broken fibers naturally lead to a build up in stress concentrations on the surrounding fibers, as demonstrated clearly in previous papers.

The simulation model starts with a completely undamaged array of fibers. As the applied load is increased, fiber breaks and associated slip occur, and the stresses are transferred to other fibers. The other fibers may break under the higher loads, and then transfer their loads onto yet other unbroken fibers. Mechanical equilibrium is established when the local loads on each fiber (applied plus transferred) are less than the local fiber strengths. At some critical applied load, however, mechanical equilibrium can never be established as all of the fibers break at least once within a slip-length of some cross-sectional plane along which the composite separates into two pieces. Since the matrix tensile load bearing capacity and the fiber volume fraction are implicit in the numerical model, the output of the model is a specific value for fiber bundle strength $\sigma_f^*$. In LLS, it proves convenient to use the characteristic strength $\sigma_c$ arising in GLS as a normalizing parameter for strengths. The fiber bundle strength depends on both the specific initial distribution of fiber strengths in the tested composite and the physical size (length and number of fibers) in the composite.

## 2.4 Analytic Local Load Sharing (LLS)

An important aspect of any model including local load sharing is the predicted size scaling of strength. Ibnabdeljalil and Curtin (1998) have recently developed an analytic model for the strength scaling under LLS, which is based on a detailed analysis of the numerical simulation results and some fascinating connections between the failure under LLS and GLS conditions. They showed that the critical cluster size in the LLS simulations could be compared to a bundle of the same size undergoing GLS, and then derived analytic asymptotic results for the strength and reliability of moderate-size (much larger than coupon size) composites under LLS, based on the failure of the constituent bundles.

In the LLS analytic model, the composite is conceptually viewed as consisting

of a collection of small fiber bundles of length $\delta_l = 0.4\delta_c$ and $n_l$ fibers in the cross-section. A volume of $N$ fibers in a length $L$ thus consists of $\mathcal{MN}$ small fiber bundles, where $\mathcal{M} = L/\delta_l$ and $\mathcal{N} = N/n_l$. The size $n_l$ is (empirically) related to the fiber Weibull modulus by

$$n_l(m) = 403m^{-1.28} \qquad 2 \leq m \leq 10 \tag{2.4}$$

At any fixed size, the strength distribution is found to be a Weibull distribution and the characteristic mean strength of a composite of volume $NL$ is predicted to be

$$\bar{\sigma} = \tilde{\sigma}\,\Gamma\left(1 + \frac{1}{\tilde{m}}\right) \tag{2.5}$$

with Weibull scale parameter

$$\tilde{\sigma} = \mu^* - \gamma^{**}\sqrt{2\log \mathcal{MN}}\left(1 - \frac{\log\left(\log\left(\mathcal{MN}\right)\right) + \log\left(4\pi\right)}{4\log\left(\mathcal{MN}\right)}\right) \tag{2.6}$$

and a composite Weibull modulus of

$$\tilde{m} = \frac{\tilde{\sigma}}{\gamma^{**}}\sqrt{2\log\left(\mathcal{MN}\right)} \tag{2.7}$$

where $\Gamma(\bullet)$ is the Gamma function. The parameters $\mu^*$ and $\gamma^{**}$ are the strength and its standard deviation, respectively, of a bundle of size $n_l$ fibers failing under Global Load Sharing, and are reproduced from Ibnabdeljalil and Curtin (1998) in Table 2.1. This model has been shown to reproduce the LLS simulation results with very high accuracy.

## 2.5 Modified Batdorf

Some years ago, Batdorf (1982) proposed a simple cumulative local damage model for predicting failure in unidirectional fiber composites. The Batdorf model followed from some earlier more-detailed asymptotic analyses by Harlow and Phoenix (1981), but was framed in a manner suitable for easy computations. Following the Batdorf analysis with a few minor modifications, we produce an analytic model corresponding closely to the LLS model for failure. Essentially, this Batdorf model is an approximation to the LLS simulation model.

The Batdorf model considers damage to occur in the form of isolated compact planar clusters of breaks which grow under increasing applied load due to stress concentrations at the edges of the cluster (Batdorf, 1982). Conceptually, the model calculates (i) the expected number of single isolated fiber breaks, $Q_1$, in a volume $V$

**Table 2.1** Global Load Sharing results for the mean strength $\mu^*$ and standard deviation $\gamma^{**}$ for the intrinsic link of size $n_l \cdot \delta_l$, for various Weibull moduli $m$.

| $m$ | $n_l$ | $\mu^*$ | $\gamma^{**}$ |
|---|---|---|---|
| 2.0 | 166 | 0.68687 | 0.02307 |
| 3.0 | 99 | 0.69961 | 0.02572 |
| 4.0 | 68 | 0.72563 | 0.02781 |
| 4.5 | 59 | 0.74149 | 0.02850 |
| 5.0 | 51 | 0.74416 | 0.02934 |
| 5.5 | 45 | 0.75161 | 0.02998 |
| 6.0 | 41 | 0.75945 | 0.03028 |
| 6.5 | 37 | 0.76763 | 0.03074 |
| 7.0 | 33 | 0.77596 | 0.03138 |
| 7.5 | 31 | 0.78318 | 0.03139 |
| 8.0 | 28 | 0.79090 | 0.03192 |
| 8.5 | 26 | 0.79788 | 0.03211 |
| 9.0 | 24 | 0.80474 | 0.03240 |
| 9.5 | 23 | 0.81062 | 0.03223 |
| 10.0 | 21 | 0.81727 | 0.03265 |

under applied stress $\sigma$, (ii) the number of isolated breaks which will grow to become a cluster of two breaks at the same stress $\sigma$ because of stress concentrations on the neighbors of the first break, (iii) the number of two-break clusters which then grow to three-break clusters, and so on. At any fixed stress, the number $Q_i$ of each cluster size $i$ is determined. The typical largest cluster at any applied stress is that size $i$ for which $Q_i \approx 1$, i.e. there is about 1 cluster of this size in the entire volume. Failure occurs at that stress for which the largest size cluster (some size $i^*$) will grow with probability unity to size $i^* + 1$ with no increase in applied stress, which will then grow to size $i^* + 2$, and so on until the cluster spans the entire system. Thus, there is a critical point in the theory at which the largest cluster becomes unstable to growth.

The calculation of the number $Q_i$ of $i$-break clusters (coined i-plets by Batdorf) proceeds as follows. Suppose at stress $\sigma$ there are $Q_i$ i-plets, each of which has $n_i$ immediate neighbors around its perimeter which are experiencing stress concentrations of $c_i$ in the plane of the breaks. Suppose further that the stress on each neighbor decays linearly, due to slip along the broken fibers, from the value of $c_i\sigma$ to the far-field value $\sigma$ over some length $\delta_i/2$. Then, the probability of failure of a single neighboring fiber can be found by integrating the Weibull probability of

failure over the length experiencing the overstress as

$$p_i = \frac{c_i^{m+1} - 1}{(c_i - 1)(m+1)} \frac{\delta_i}{L_o} \left( \frac{\sigma}{\sigma_o} \right)^m \quad . \tag{2.8}$$

Since each neighbor has this probability of failure, the number of $Q_{i+1}$ clusters formed from the $Q_i$ clusters is simply

$$Q_{i+1} = Q_i n_i p_i \quad . \tag{2.9}$$

The initial starting point for this iterative evolution of break clusters is the number of expected 1-plets in the entire volume of the material,

$$Q_1 = N(1 - e^{-\frac{L}{L_o}(\frac{\sigma}{\sigma_o})^m}) \approx N \frac{L}{L_o} \left( \frac{\sigma}{\sigma_o} \right)^m \tag{2.10}$$

where the approximation is accurate if $Q_1 \ll NL/\delta_1$, which is always the case.

At any stress $\sigma$, the above scheme generates a set of $\{Q_i\}$ values. The point of failure is then found as that stress at which there is a cluster size $i^*$ which simultaneously satisfies the conditions

$$Q_{i^*} = 1 \tag{2.11}$$

$$Q_{i^*+1} > Q_{i^*} \tag{2.12}$$

The first condition states that there is typically one cluster of size $i^*$ in the entire system. The second, critical, condition states that the $i^*$ system is actually unstable to growth to size $i^*+1$ at the current stress. Both conditions are necessary for failure to occur. The stress $\sigma$ at which failure is calculated from Eqs. 2.8–2.12 is precisely the fiber bundle failure stress $\sigma_f^*$ in Eq. 1.13, and the UTS follows from Eq. 1.13.

To make explicit connection with our simulation results, and the expected mechanics of the debonding and sliding interface in Ti-MMCs, we proceed as follows. First, the fibers are arranged in a square array. The clusters of planar breaks are chosen to be nearly circular and the stress concentration factors for planar clusters of fiber breaks are as obtained from our simulations, which are identical to those given by Hedgepeth and van Dyke (1967). These choices are also identical to those used previously by Batdorf and Ghaffarian (1982), and the relevant values of $n_i$ and $c_i$ are shown in Table 2.2. Finally, the length $\delta_i/2$ is chosen to be the slip length at the current stress level, independent of the cluster size $i$, so that

$$\delta_i = \frac{r\sigma}{\tau} = \delta_c \left( \frac{\sigma}{\sigma_c} \right) \quad . \tag{2.13}$$

**Figure 2.2** Evolution of failure in the Batdorf model. Breaks form at successive levels of stress from local stress concentrations due to other breaks.

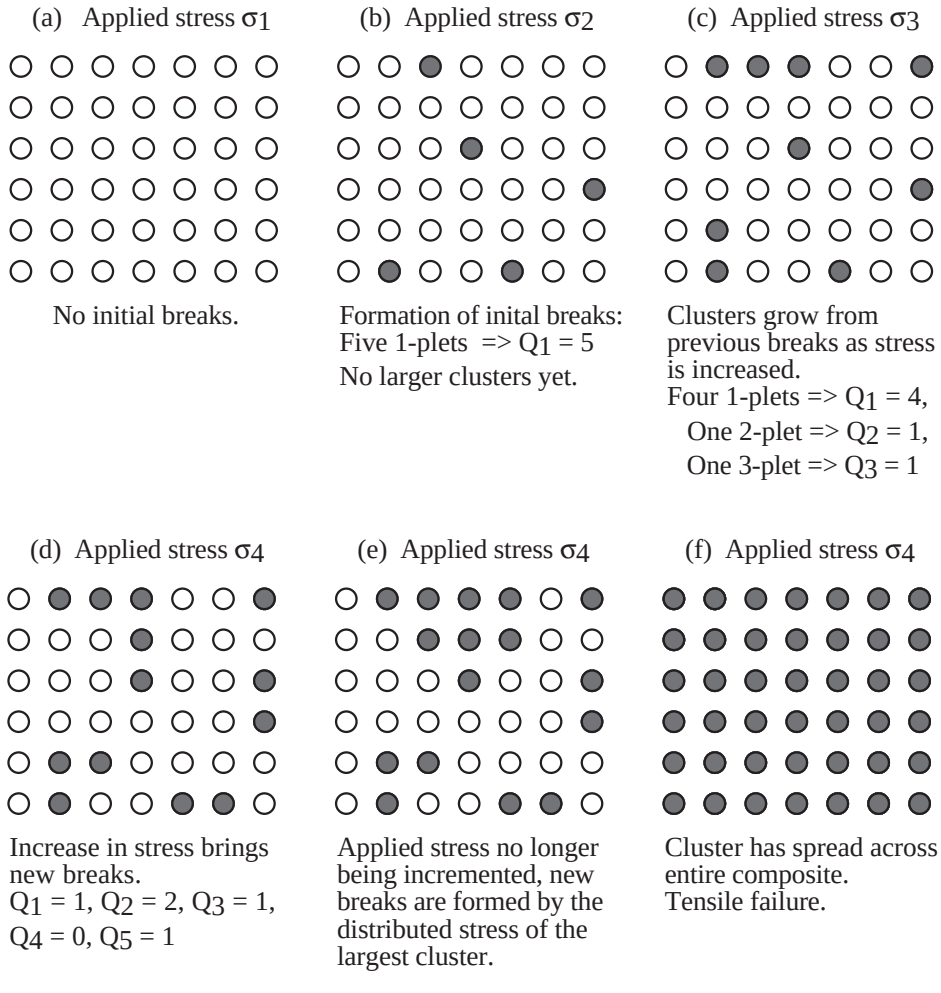

**Table 2.2** Number of near neighbors $n_i$ and stress concentration factor $c_i$ on those neighbors, for various clusters of near-circular fiber breaks up to $i$=12 and for square arrays of fiber breaks of size $i$ for $i > 12$.

| $i$ | 1 | 2 | 3 | 4 | 5 | 6 | 7 | 8 | 9 | 10 |
|---|---|---|---|---|---|---|---|---|---|---|
| $c_i$ | 1.146 | 1.18 | 1.225 | 1.281 | 1.31 | 1.34 | 1.375 | 1.405 | 1.456 | 1.46 |
| $n_i$ | 4 | 6 | 7 | 8 | 9 | 10 | 11 | 11 | 12 | 13 |
| | | | | | | | | | | |
| $i$ | 11 | 12 | 16 | 25 | 36 | 49 | 64 | 81 | 100 | |
| $c_i$ | 1.48 | 1.5 | 1.582 | 1.728 | 1.841 | 1.975 | 2.083 | 2.2 | 2.303 | |
| $n_i$ | 14 | 15 | 16 | 20 | 24 | 28 | 32 | 36 | 40 | |

This condition on $\delta_i$ leads to the same slip lengths as used in the LLS simulation model. Substituting this result into Eq. 2.8, and introducing the normalizing parameters $\sigma_c$ and $\delta_c$ for stress and length, respectively, the final result for the number of $Q_i$ breaks clusters at stress $\sigma$ is given by

$$Q_i = \frac{NL}{\delta_c}\left(\frac{\sigma}{\sigma_c}\right)^{i(m+1)-1} \prod_{j=1}^{i-1} \frac{n_j(c_j^{m+1}-1)}{(c_j-1)(m+1)} \quad , \tag{2.14}$$

which is obtained by combining Eqs. 2.8–2.10. Note that we have normalized stress by $\sigma_c$ and the length by $\delta_c$, just as in the GLS and LLS models. The Pi-product in Eq. 2.14 is also dimensionless, and is simply a function of $i$ and $\sigma$ for a given set of neighbors $n_i$ and stress concentrations $c_i$. Calculating the $Q_i$ values from Eq. 2.14 and applying the failure conditions of Eqs. 2.11–2.12 leads to predictions for the composite strength.

## 2.6 Comparison of Modified Batdorf and LLS models

The two models use the same fiber geometry, and the stress concentrations for planar arrays of breaks are identical. However, the simulation model accounts for the actual longitudinal location of the fiber breaks, and hence pullout and a smearing of the stress concentration factors; this would tend to increase the predicted strength. The simulation model also distributes stress to further neighbors beyond the immediate perimeter, allowing for more damage and coalescing of damage; this would tend to decrease the predicted strength. The Batdorf model permits just one cluster shape of each size and uses an average stress concentration factor along the perimeter, whereas complex cluster shapes and local stress concentrations arise quite naturally

in the simulation model; these suggest lower strengths in the simulation model. In the Batdorf model, the probability of fiber breakage is calculated based on an overstressed region of $\pm\delta_i/2$ but then the break itself is placed in the same physical plane as the previous breaks in the cluster. The fibers are therefore all broken in the same plane and there is no pullout, or remaining fiber load carrying capability, after a fiber breaks. In the LLS model, the 3D character of the fiber breakage is explicitly included. At higher Weibull moduli, there are shorter pullout lengths and less fiber damage prior to failure, so that the pullout contribution of the broken fibers to the composite strength is small. At lower Weibull moduli, the pullout makes an important contribution to the strength. In the Batdorf model, the total applied force is not conserved: the total force redistributed from a broken fiber to the neighboring fibers is less than the force on the fiber, which increases the strength prediction. From these points, it is clear that the Batdorf model developed here corresponds to an approximation of the LLS simulation model. To create an analytic model, Batdorf has eliminated certain more-complicated aspects of the failure that are naturally included in the LLS simulation model. Below, we study the size scaling of the two models in more detail to check the general agreement over a range of composite sizes and a broad range of Weibull moduli, and find that important differences do exist between the LLS model and the more-approximate Batdorf model.

### 2.6.1 Size Scaling

*By a small sample we may judge the whole piece.*
—Miguel de Cervantes, *Don Quixote*

An important aspect of any model including local load sharing is the predicted size scaling of strength. Here, we analyze in more detail the Batdorf model predictions for tensile strength versus composite size and fiber Weibull modulus, and compare them in detail to the analytic LLS model (which yields predictions identical to those obtained in the LLS simulations).

In the Batdorf model, the calculated strength is the characteristic strength as well, but the results are not expressible in a simple analytic form. The central portion of the strength probability distribution is also predicted to be Weibull in form with a Weibull modulus of $mi^*$, where $i^*$ is the size of the critical cluster of fiber breaks. Determination of the strength and Weibull modulus versus size proceeds by direct calculation from Eqs. 2.3 - 2.10 above after specific input of the size $NL$.

Figures 2.3a, 2.3b and 2.4 show the dimensionless fiber bundle strength $\sigma_f^*/\sigma_c$ versus dimensionless composite size ($NL/\delta_c$), as predicted by the Batdorf and LLS models for fiber Weibull moduli of $m = 2$, 5, and 10 respectively. Discontinuities in the Batdorf models arise because neighboring size ranges will have different values

**Figure 2.3** Normalized fiber bundle strength $\sigma_f^*/\sigma_c$ versus normalized composite volume $(NL/\delta_c)$ as predicted by the Batdorf-type model and the LLS analytic model of Ibnabdeljalil and Curtin, for fiber Weibull moduli of (a) $m$=2 and (b) $m$=5.

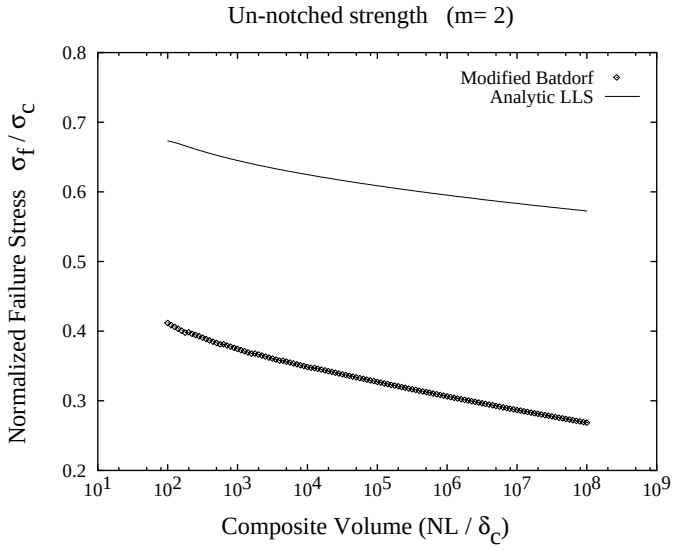


(a)

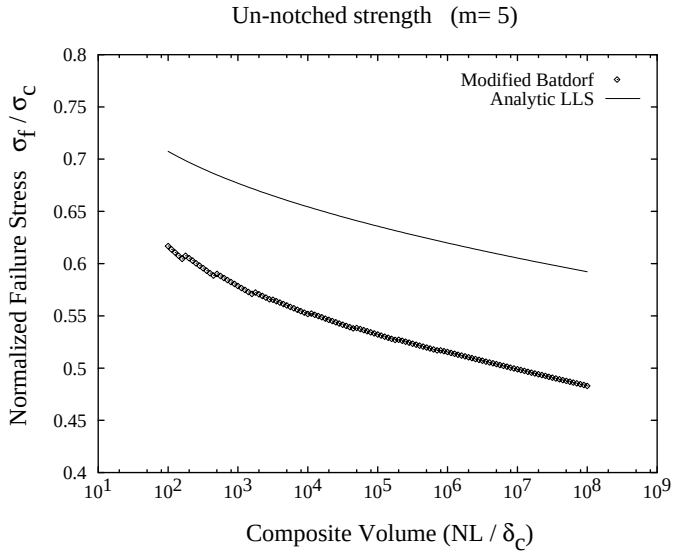


(b)

**Figure 2.4** Normalized fiber bundle strength $\sigma_f^*/\sigma_c$ versus normalized composite volume $(NL/\delta_c)$ as predicted by the Batdorf-type model and the LLS analytic model of Ibnabdeljalil and Curtin, for fiber Weibull moduli of $m = 10$.

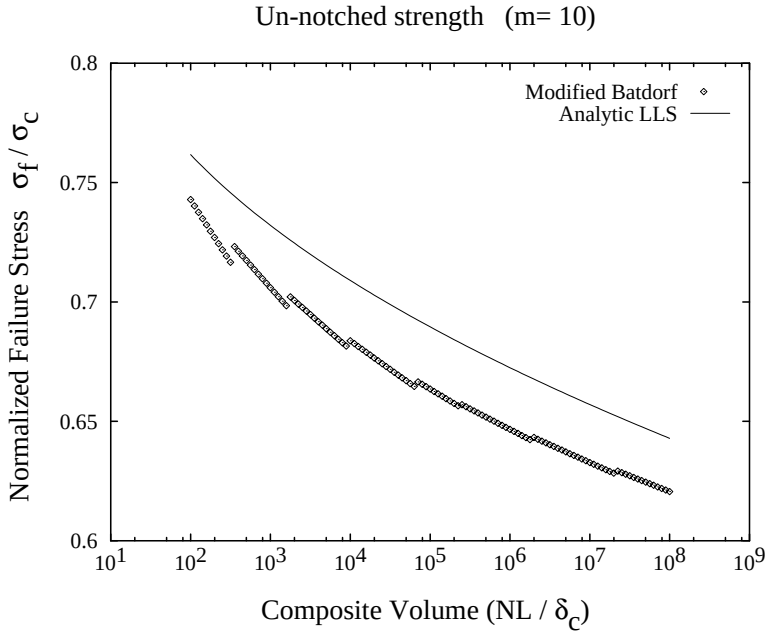


for the critical cluster size leading to failure. These artifacts become less pronounced as size is increased or Weibull modulus decreased. Neglecting the discontinuities in the Batdorf predictions, the two models agree on the general trend of behavior. The two models also agree quantitatively for high Weibull moduli. The discrepancies become glaring as $m$ is reduced, however, and for $m = 2$ the Batdorf model severely underestimates the composite strength. Since $m$ = 2-5 is a typical range for many fibers, the Batdorf model should not be used in such cases. In spite of the overall differences in magnitude, the predicted scalings of strength with composite size are remarkably similar. The origins of this similarity are not yet understood however. These results suggest the Batdorf model can be used reliably at higher $m$, $m \geq 10$, and over a wide range of sizes.

### 2.6.2 Notch Strength

*So may a glory from defect arise.*

—Robert Browning, *Deaf and Dumb*

A second comparison between the Batdorf and simulation models can be made by considering their respective predictions of "notch strength". Ibnabdeljalil and

Curtin (1998) have recently presented simulations of composite failure in the presence of an initial "notch" consisting of a square planar array of broken fibers . Failure around such notches was found to depend on the stress concentration around the notch and the extent of fiber pullout, which is strongly dependent on fiber Weibull modulus. In terms of the notation used here, the normalized notch strength of the composite was found to be

$$\sigma = \frac{\mu^*}{c_i} + \sigma_p \tag{2.15}$$

where the normalized pullout stress $\sigma_p$ is given by

$$\sigma_p = \left(\frac{1}{m+1}\right)^{\frac{m}{m+1}} \Gamma\left(\frac{m+2}{m+1}\right) \tag{2.16}$$

and $\mu^*$ is the strength of the critical link at the notch as tabulated in Table 2.1.

In the Batdorf-type analysis, an initial notch of size $i_n$ can be introduced by simply setting $Q_{i_n} = 1$ at the outset. Failure due to such an initial notch then occurs when the notch begins to grow unstably, i.e. when $Q_{i_n+1} = 1$. Damage occurring elsewhere in the system evolves separately and need not be considered in this model. From the Batdorf analysis of Eq. 2.9, we see that the failure emanating from an initial notch of size $i_n$ occurs when

$$Q_{i_n} = Q_{i_n+1} = 1 = n_{i_n} p_{i_n} \tag{2.17}$$

Solving this condition for the stress yields the notch strength of

$$\sigma_f^* = \left(\frac{(c_{i_n}-1)(m+1)}{n_{i_n}(c_{i_n}^{m+1}-1)}\right)^{\frac{1}{m+1}} \tag{2.18}$$

The required values of $n_{i_n}$ and $c_{i_n}$ for large notches are not contained in (Batdorf, 1982) and (Batdorf and Ghaffarian, 1982). However, for square notches of size $i_n$, the stress maximum stress concentration factors have been calculated in (Ibnabdeljalil and Curtin, 1997) and are also shown in Table 2.2. The number of near neighbors $n_i$ is taken simply as $4n_i$, which neglects the neighbors on the corners of the square notch.

The predicted notch strengths from the Batdorf and LLS models are shown in Figure 2.5 for Weibull moduli of $m = 5$ and 10. For $m = 10$, the model predictions are nearly parallel, with a modest (10%) difference in magnitude. For $m = 5$, however, there is a much larger difference in the predicted behaviors. The Batdorf model predicts a much more rapid weakening of the notch strength with increasing notch size than predicted by the LLS model or seen in the LLS simulations. Furthermore, the Batdorf model predicts that the $m$=5 strengths are always below the $m$=10

**Figure 2.5** Normalized fiber bundle notch strength $\sigma_f^*/\sigma_c$ versus initial notch size $i_n$, as predicted by the Batdorf-type model and an LLS analytic model of Ibnabdeljalil and Curtin (IC), for fiber Weibull moduli of 5 and 10. Note that the Batdorf-type model predicts that m=5 is always weaker than m=10, in contrast to the predictions of the LLS model.

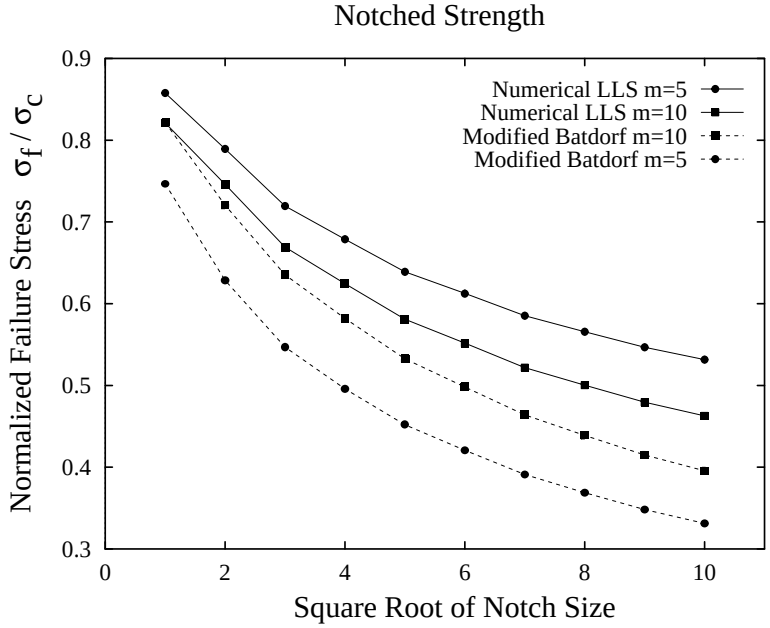


strengths out to notch sizes of $i_n$=10, whereas the LLS model and simulations show that the $m$=10 materials are weaker, particularly for larger notch sizes. This differing behavior can be traced to fiber pullout. The fiber pullout stress, absent in the Batdorf model, acts as a tremendous stabilizing influence at larger notch sizes and ultimately dominates the notch strength and composite toughness, as physically expected and observed in Ti-MMCs. Using the Batdorf model for guidance in composite design would thus suggest that high-Weibull fibers are preferable for both high strength and high toughness, which is not really the case. High Weibull fibers provide higher unnotched strengths (see Figs. 2.6.1–2.4) but do sacrifice toughness, or notch strength, as observed in the LLS model.

Thus, in spite of the reasonable success of the Batdorf-type model in predicting un-notched tensile strength at higher Weibull moduli, it is not very accurate in assessing either the magnitude or trends in notch strength of composites operating under LLS.

## 2.7 Summary

Using much of the formalism and some of the assumptions associated with the Global Load Sharing model, we have developed an analytic Batdorf-type model, which is an approximation to the Local Load Sharing simulation model. The Batdorf model agrees with an analytic model derived from the simulation on the general trends of scaling of strength with composite size, but differ in the actual strength predictions, especially at lower Weibull moduli. A comparison of predicted notch strength also shows marked difference between the Batdorf-type and simulation-based models.

# Chapter 3

# Boundary Effects and Heterogeneous Loads

*A computer lets you make mistakes faster than any other invention in human history, with the possible exception of handguns and tequila.*
—D.W. McArthur

We will now investigate the effects of free boundary conditions (as opposed to periodic boundary conditions) in the fiber lattice on the numerical LLS model. The method used leads naturally to a method of simulating disordered arrays of fibers, as opposed to regular square arrays. To achieve a valid comparison, a square lattice with the same number of fibers and the same mean fiber spacing must be created. The use of free boundaries is also required, in part, to investigate the effects of certain non-constant load gradients, specifically the load gradients resulting from bend-testing. We will further modify the Batdorf model to include the effects of varying load gradients.

## 3.1 Motivation

The basic numerical LLS model utilizes a Green's function technique to communicate load redistribution between fibers. The use of a periodic lattice becomes the most natural and efficient way to execute this method. A small lattice with periodic boundary conditions better mimics the interior behavior of a much larger system such as those used in real applications. While ignoring boundary effects may not be entirely valid when used to look at small test coupons, the assumption has been that the difference between periodic and free boundary conditions is minimal on the overall simulated strength of the composite. Since some samples (in fact all the Ti-MMC coupons investigated in this work) are small enough that it becomes tractable

to simulate all the fibers in the composite and include free boundary effects, this seems a good time to reexamine that assumption. Testing this assumption was one factor in implementing free-boundary modifications, but secondary to the desire to implement free-boundary techniques for non-constant loads, specifically those whose gradients did not have periodic values, i.e. under bending, the extremes (minimum and maximum) of the stress gradient are at the top and bottom of the test specimen.

## 3.2 Modeling Procedure and Boundary Effects

In the numerical LLS model the easiest way to model areas devoid of fibers is to simply completely break (break at each discretization along the entire length) the fibers at that location; the result is that no stress can be carried at the locations occupied by the broken fiber. Thus redistributed loads that would have been carried by those fibers go to nearby intact fibers. In the case of modeling a free boundary, the general idea is to create a buffer of completely broken fibers, usually 4 to 8 fibers wide. This method proves fairly successful; a new fiber break attempting to redistribute its load across this "dead zone" will have less than 8% of the total redistributed stress "leak" through the dead zone in the worst case of a fiber break at the boundary. While this method is the easiest to implement, for an algorithm whose computational time depends on the number of breaks, this can become computationally expensive. It is this expense that motivates some of the concern to look for differences in the strength results of periodic vs. free-boundary systems.

Under LLS rules, fibers sufficiently far from the edges of a composite with free boundaries should behave identically to fibers in a periodic composite; the range of the load sharing should not "see" the edges of the composite. So if failure originated in the center of the composite and worked its way to the edges symmetrically, the overall effects should be the same. However damage forming near the edges is constrained by the geometry of the composite to spread towards the center and along the edges, it can not cross to the other side as it would under periodic conditions. This may in fact limit the spread of damage. Since the damage spreads when nearby fibers are overloaded by the redistributed stress, of interest are fibers that are subject to larger than average amounts of stress. Specifically, fibers which break at the edges have only three nearest neighbors (as opposed to four) and those at the corners have only two. Fibers that break in this location shunt the bulk of their load to far fewer fibers than fibers that break away from the boundaries of the composite.

With out investigating, it is unknown whether these effects may hasten, limit, or have negligible effect on the spread of damage. An example of the stress redistribution generated by the numerical LLS simulation in a layer for a fiber broken at the edge of a composite is shown in Figure 3.2. A similar example for stress

**Figure 3.1** Example of stress redistribution due to a break away from a boundary. Fraction of load transferred from break is shown. The 4 nearest neighbors carry 58.4% of the total redistributed load. Approximately 7% of the load is transferred beyond the region of the composite shown.

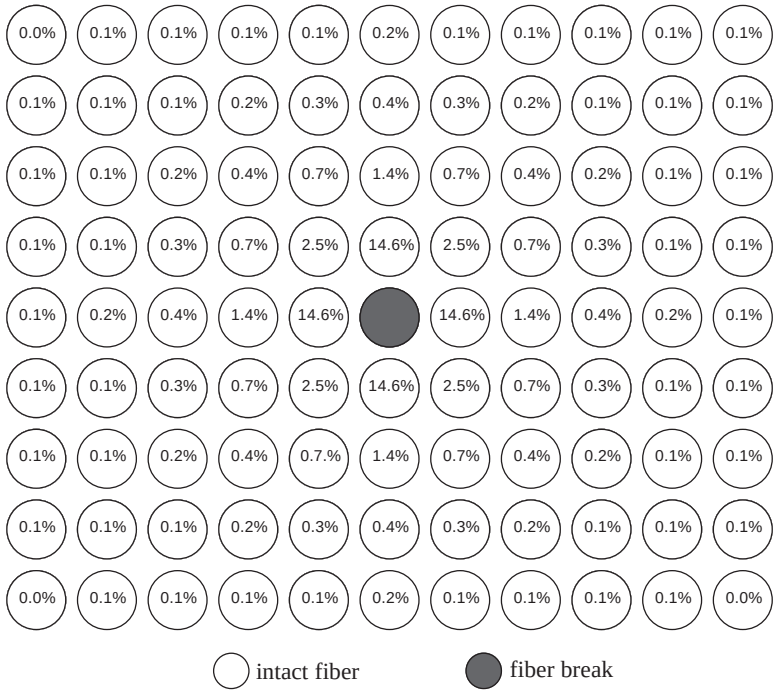

**Figure 3.2** Stress redistribution due to a break at a free boundary. Approximately half of the transferred load is carried by the three nearest neighbors.

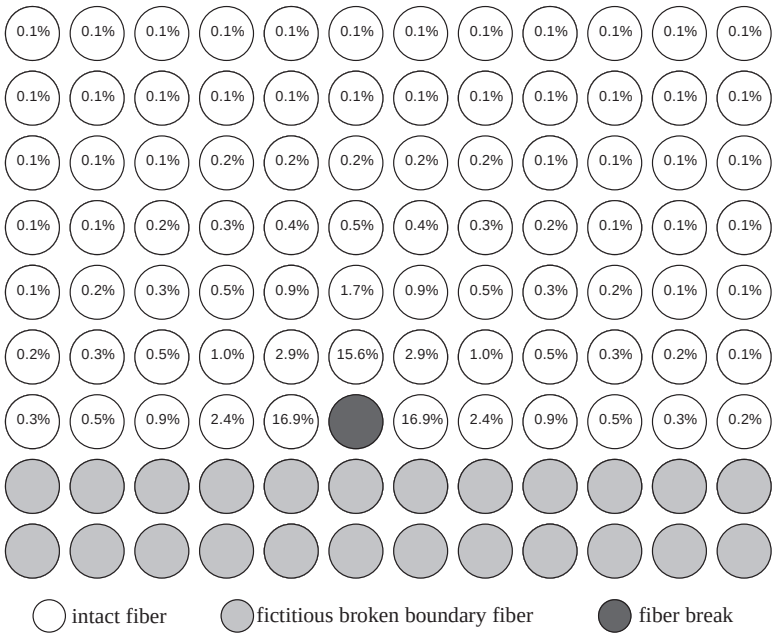


redistribution originating from the corner is shown if Figure 3.3. This can be compared to the stress redistribution by a break that is able to communicate load to all nearby fibers as shown in Figure 3.1. It is interesting to note that although stress on the nearest fibers is much greater for breaks at the edge and corner, it not a simple multiplicative increase; i.e. even though a break at a corner has only half the nearest neighbors of a break in a periodic system, the transferred load to nearest neighbors is much less than double what is transferred to nearest neighbors for the unbounded system break.

This stress redistribution does not just occur at fiber breaks; when a fiber breaks, the resulting pieces undergo "slip" as previously discussed. Thus along the slip length in both directions around the break, the fibers carry less than the far-field load and the remaining stress is redistributed in each layer using the same load sharing rules.

## 3.3 Results: Periodic vs. Free Boundary

In Chapter 4 we will compare the strength predictions of the numerical LLS model to the experimental results performed by Gundel and Wawner (1997). The fiber

**Figure 3.3** Stress redistribution due to a break at the corner of free boundaries. Approximately 36.8% of the transferred load is carried by the two nearest neighbors.

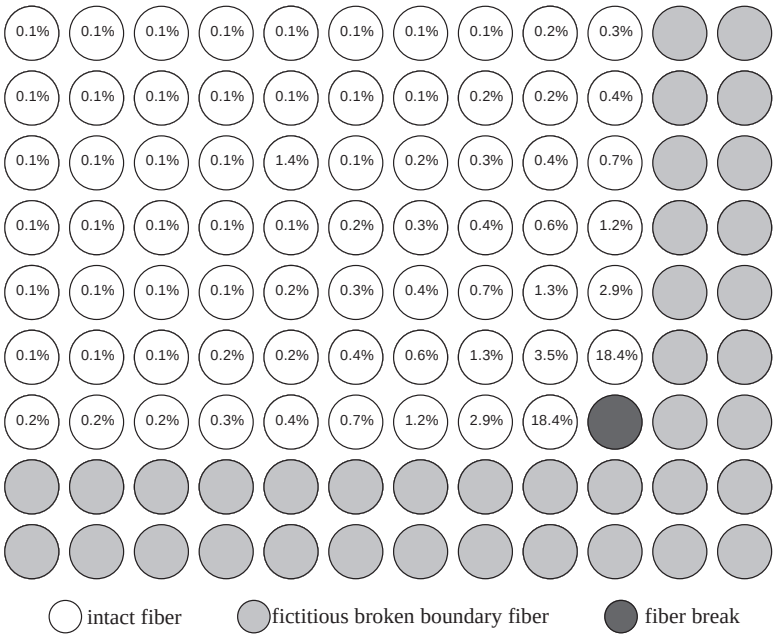


geometry of the experimental coupons used consisted of a 4x26 lattice of fibers. We will use the same geometry to examine periodic and free-boundary differences in the model. In addition to the periodic and completely free boundary systems, we will also look at a "semi-free" system, where the long (26 fiber) border of the system will have a free boundary and the short (4 fiber) border will maintain the periodic boundary condition. Effectively the periodic system models an infinite planar array of fibers and the semi-free system models an infinite strip, 4 fibers in width. To create the semi-free system, a 4x30 lattice is created and a two fiber wide "moat" of broken fibers is formed on either side of the composite, leaving a 4x26 lattice of intact fibers inside as shown in Figure 3.4. Similarly for the completely free boundary system, an 8x30 lattice is created with a two fiber wide "moat" completely surrounding a 4x26 lattice of intact fibers as shown if Figure 3.5.

Since composite length (fiber length) will vary for various samples, we will use a common length of $2\delta_c$ in our investigations. Any strength changes due to the boundary conditions should scale with the length. Weibull moduli of $m = 2$, 5, 10, and 20 were used and 100 simulations were performed for each geometry and Weibull modulus. These results are shown in Table 3.1. Uncertainty in the standard deviation of the mean fiber bundle strength is $1/\sqrt{2(100-1)} = 7.1\%$. For a given Weibull modulus, the mean fiber bundle strengths are well within a standard

**Figure 3.4** Semi-free boundary cross section. Border of broken fibers around intact fibers attempts to effect a free boundary on that surface while leaving sides with periodic conditions.

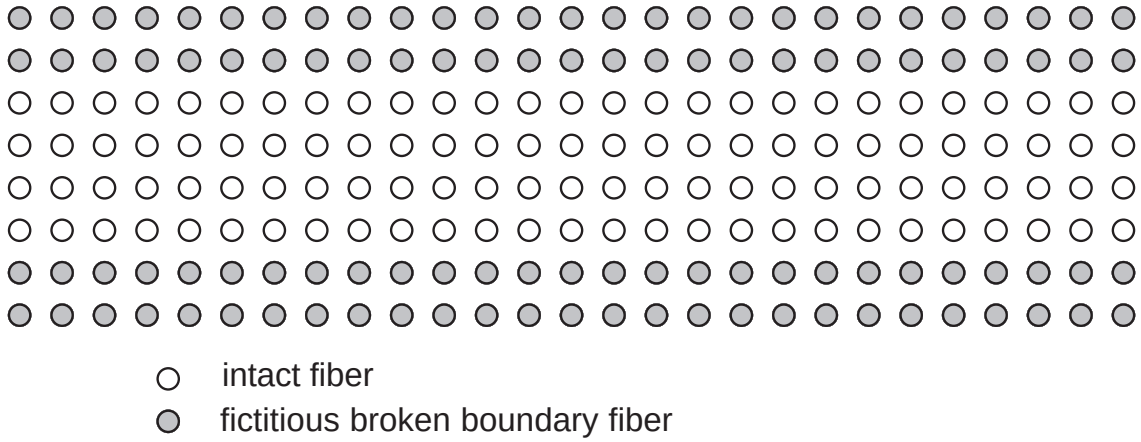


**Figure 3.5** Free boundary cross section. Border of broken fibers around intact fibers attempts to effect free boundary conditions.

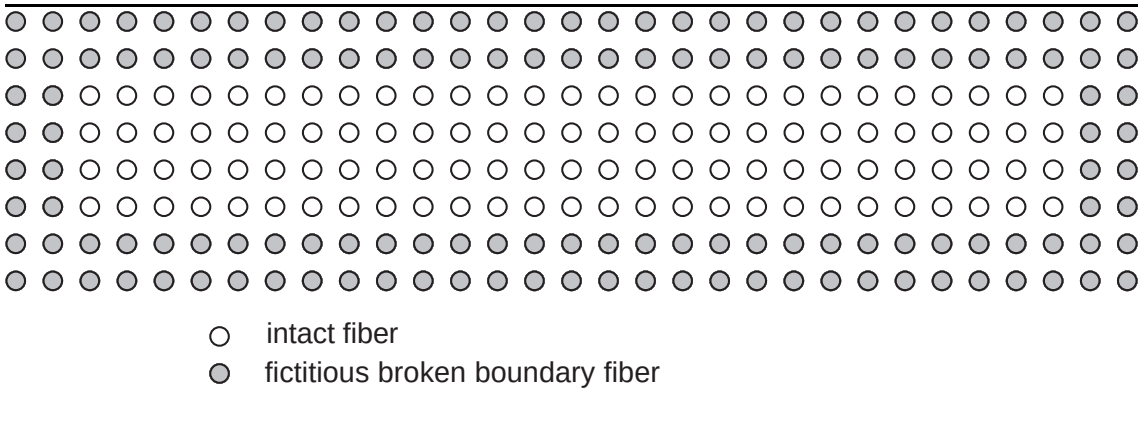

**Table 3.1** Fiber-bundle strengths (in units of characteristic stress $\sigma_c$) of 100 simulated composites having free, semi-free, and periodic boundary conditions at various Weibull moduli. Composite configuration consisted of a 4x26 array of fibers of length $2\delta_c$.

Fiber Bundle Stength (mean ± std dev)

| | Weibull Modulus | | | |
|---|---|---|---|---|
| Simulation Geometry | 2 | 5 | 10 | 20 |
| Periodic | 0.650 ± 0.026 | 0.678 ± 0.022 | 0.740 ± 0.022 | 0.803 ± 0.022 |
| Semi-free | 0.653 ± 0.025 | 0.691 ± 0.018 | 0.748 ± 0.018 | 0.807 ± 0.027 |
| Free | | 0.686 ± 0.020 | 0.750 ± 0.018 | 0.803 ± 0.024 |

deviation of one another. This makes clear that for a given Weibull modulus, there is no statistically significant difference in the ultimate fiber bundle strength due to boundary effects for this 4x26 geometry.

## 3.4 Random Fiber Arrangements

Up to this point the only arrangement of fibers that has been considered has been ordered fibers in a square lattice. Of interest is the strength of composites with spatially-distributed fibers, specifically random arrays of fibers. The fibers are still unidirectional, but the locations within a cross section perpendicular to the fiber direction have been randomly generated. Obviously this is of interest when considering that real components are not manufactured as perfect lattices. Here we look at lattices that have had 50% of the fibers removed to create a disordered microstructure.

In a random structure, you might tend to find "lonely" fibers: fibers with few near neighbors. When breaks occurs in sparsely populated neighborhoods, the stress concentrations on remaining fibers tends to be much greater than in more heavily populated neighborhoods. This is very similar to a break occurring at the corner of a free boundary; only a limited number of nearby fibers are available to carry the transferred load. Some examples of the stress redistribution in random lattices due to a fiber break are shown in Figure 3.6 and Figure 3.7.

Obviously when we consider a composite that is missing half of its fibers, it will

**Figure 3.6** Example of stress redistribution due to a break in a random lattice with a locally high concentration of fibers.

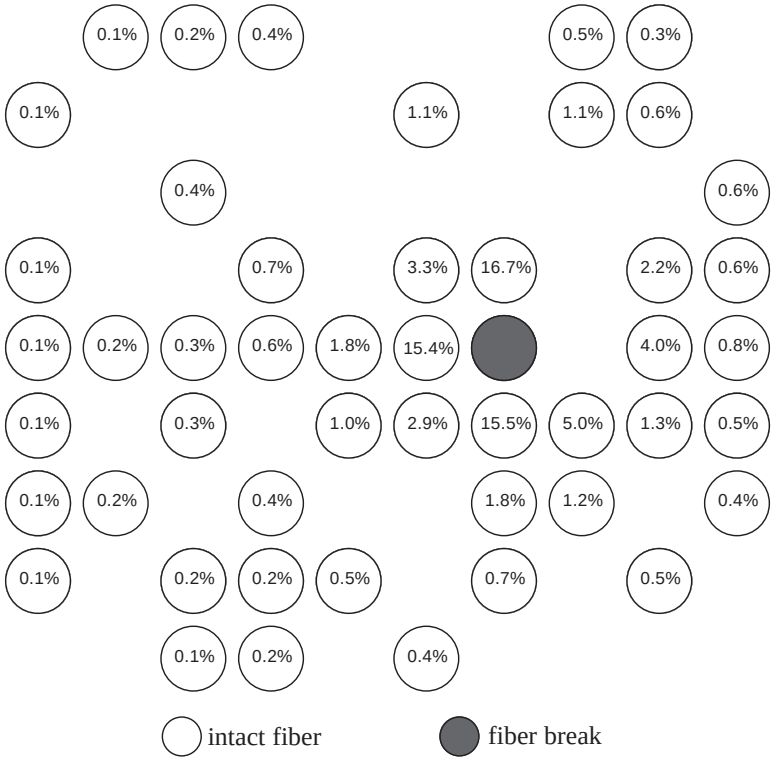

**Figure 3.7** Example of stress redistribution due to a break in a random lattice with a lower concentration of fibers in the immediate vicinity of the break.

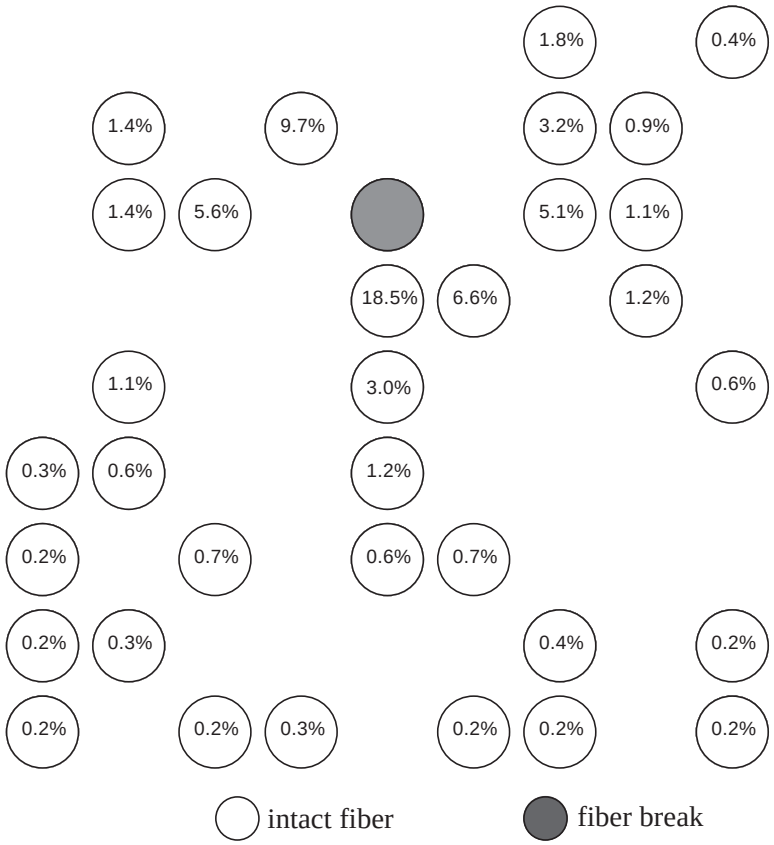

not be as strong as a composite with the same dimensions but twice the fibers. However we can not simply compare the strength results with an ordered lattice that has same number of fibers, since the fiber density, and therefore the mean fiber spacing, is not the same. The change in fiber spacing changes the load sharing rule. What is needed is an ordered lattice with the same number of fibers *and* the same mean fiber spacing. This is accomplished by removing the fibers of a composite in a checkerboard pattern, thereby removing half the fibers. If we tilt our heads 45°, we see that we still have an ordered square lattice, but we have increased the mean fiber spacing by a factor of $\sqrt{2}$ to match the random case. An example of the stress redistribution in this new lattice is shown in Figure 3.8.

**Figure 3.8** Example of stress redistribution due to a break in a checkerboard lattice; an ordered square lattice whose average fiber density is equal to that of the random case.

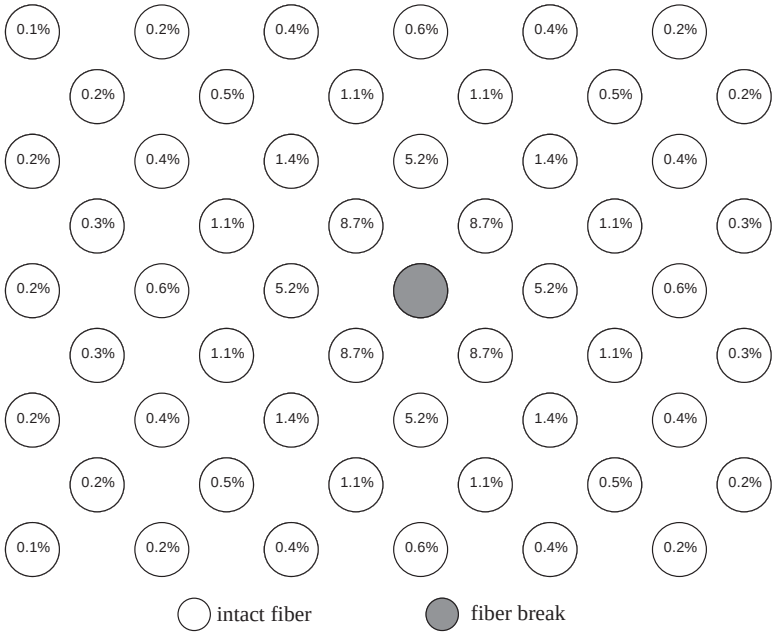


## 3.5 Results: Checkerboard vs. Random

The regular square (checkerboard) lattice used for the simulations was created by taking a 20x20 lattice and removing every other fiber, leaving 200 intact fibers. The random lattices were created by picking fibers at random to remove and repeating until 200 fibers were left. Both simulations used fiber lengths of $2\delta_c$ and 50 simula-

tions were performed on each system. It should be noted that each of the random lattice simulations was indeed done on a different random lattice. The resulting failure strengths are shown in Table 3.5.

Another representation of the strength results is shown in Figure 3.9. This plot takes the cumulative failure probability distribution versus failure stress and transforms the axis such that the $y$-axis corresponds to a Normal (Gaussian) probability curve, i.e. $\Phi^{-1}(z)$ versus stress. The effect of using such a coordinate axis is such that Gaussian distributions will plot as straight lines that intercept the stress axis at the mean failure stress of the distribution. The slope of such a line corresponds to the standard deviation of the distribution. Hence a steeper line corresponds to a less scattered distribution. The slopes of all four data sets are very similar, suggesting a similar distribution shape.

One would expect that the disordered (random) lattice would in general be weaker then the ordered (checkerboard) lattice; patches of sparse fiber distributions would weaken portions of the composite causing failure to propagate from those patches. Indeed for the higher Weibull modulus composites ($m = 10$), the ordered lattice is measurably stronger then the disordered lattice. For the lower Weibull modulus composites ($m = 5$) the strengths are indistinguishable. This is most likely due to the state of the lattices prior to failure; the lower the Weibull modulus, the more damage the composite can sustain prior to failure. Just prior to failure the damage sustained by the ordered lattice has essentially "disordered" it. A comparison of a typical failure plane for ordered and disorded lattices at $m = 5$ and 10 is shown in Figures 3.10 and 3.11.

Since a 200 fiber system corresponds to a small to medium size coupon, it is really to small to represent most real world applications. We would like to predict the strength of these systems as size increases. To do so, we assume that weak-link scaling applies as shown on other data by Ibnabdeljalil and Curtin (1998). Then the failure probability distribution $H_{n_f}(\sigma)$ of a system consisting of $n_f$ fibers, is related to that of a similar system geometry of size $n$ by,

$$H_n = 1 - \left(1 - H_{n_f}\right)^{\frac{n}{n_f}} \tag{3.1}$$

for sufficiently large $n$ and $n_f$.

Curtin (1998) showed that for a given Weibull modulus, there is a critical bundle size $n_c$ that corresponds to the critical cluster size seen in the simulations. Furthermore the failure probability distribution of this bundle corresponds exactly to a Gaussian. Large LLS systems can be viewed as failing as if they were composed of a series of $n_f/n_c$ bundles. The $n_f/n_c$ bundles fail as under GLS and the weakest of these individual bundles causes failure of the composite system. This forms the basis of the LLS analytic theory discussed in Section 2.4. The number of fiber bundles $n_f/n_c$ is equivalent to $\mathcal{MN}$ in the analytic LLS formulation. For convenience we

**Table 3.2** Fiber-bundle strengths (in units of characteristic stress $\sigma_c$) of 50 simulated composites each having a random lattice structure or a square (checkerboard) lattice with the same mean fiber population density at Weibull moduli $m = 5$ and 10 and fiber length $2\delta_c$.

Fiber Bundle Stength (mean ± std dev)

| | Weibull Modulus | |
|---|---|---|
| Fiber Distribution | 5 | 10 |
| Checkerboard | 0.697 ± 0.017 | 0.762 ±0.014 |
| Random | 0.698 ± 0.014 | 0.752 ± 0.011 |

will reproduce Equations 2.6– 2.7 and make the substitution $\mathcal{MN} = n_f/n_c$. The failure probability distribution $H_{n_f}(\sigma)$ for large sizes $n_f$ is modeled as a Weibull distribution

$$H_{n_f}(\sigma) = 1 - e^{\left(\frac{\sigma}{\tilde{\sigma}}\right)^{\tilde{m}}} \tag{3.2}$$

with Weibull scale parameter

$$\tilde{\sigma} = \mu^* - \gamma^{**}\sqrt{2\log n_f/n_c}\left(1 - \frac{\log\left(\log\left(n_f/n_c\right)\right) + \log\left(4\pi\right)}{4\log\left(n_f/n_c\right)}\right) \tag{3.3}$$

and a composite Weibull modulus of

$$\tilde{m} = \frac{\tilde{\sigma}}{\gamma^{**}}\sqrt{2\log\left(n_f/n_c\right)} \tag{3.4}$$

To use our simulation data, $H_{n_f}(\sigma)$, to predict the strength of larger composites, $H_n(\sigma)$, we must find the size $n$ that corresponds to the characteristic strength $\tilde{\sigma}$; $H_n(\tilde{\sigma}) = 1 - e^{-1}$. Combining this with Equation 3.1 and solving for $n$ yields the size $n$ having strength $\tilde{\sigma}$, we find

$$n = \frac{-n_f}{\log\left(1 - H_{n_f}(\tilde{\sigma})\right)} \tag{3.5}$$

Since we know $H_{n_f}(\tilde{\sigma})$ for a specific $n_f$ (in our checkerboard and random simulations $n_f = 200$), we can predict the strength versus size based on the strength distribution

**Figure 3.9** Cumulative failure probability distribution versus stress of random and checkerboard lattices at $m = 5$ and 10. Probability is plotted on a Gaussian axis such that Gaussian distributions plot as straight lines that intercept the stress axis at the mean.

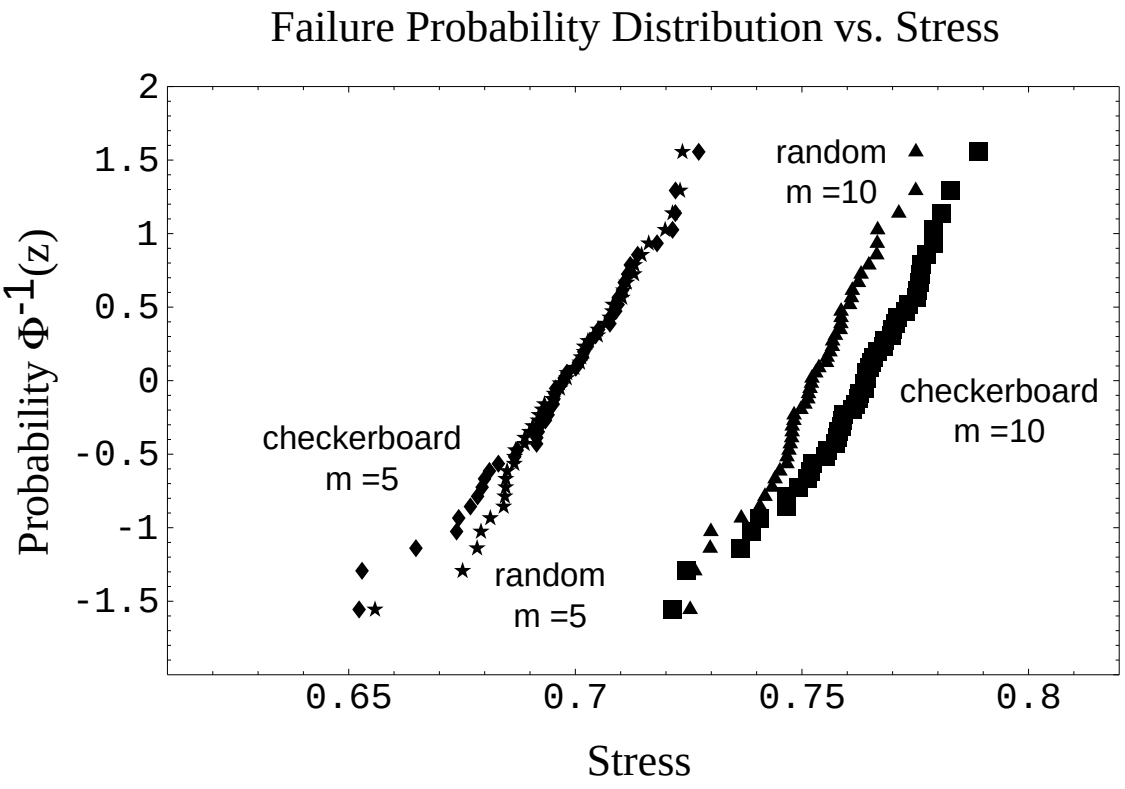


of our fixed size data as shown in Figure 3.12. Since Equations 3.3– 3.4 suggest that strength should scale as $\sqrt{\log n}$, this provides a convenient scale for visual representation. Although we would most often use such a size scaling plot to predict the decrease in strength as size increases, we are given an equal amount of information about size scaling of smaller composites. Simulation of a 10x10 checkerboard lattice (50 fibers, $\sqrt{\log 50} = 1.98$) resulted in a mean strength of approximately 0.73 $\sigma_c$ which corresponds well with the prediction of size scaling given by Figure 3.12.

**Figure 3.10** Cross section of eventual plane of failure for both ordered (checkerboard) and disorded (random) lattices for Weibull modulus $m = 5$. Both systems failed at an identical applied tensile stress of 0.698 $\sigma_c$. Note similar amount of damage to both systems at failure stress.

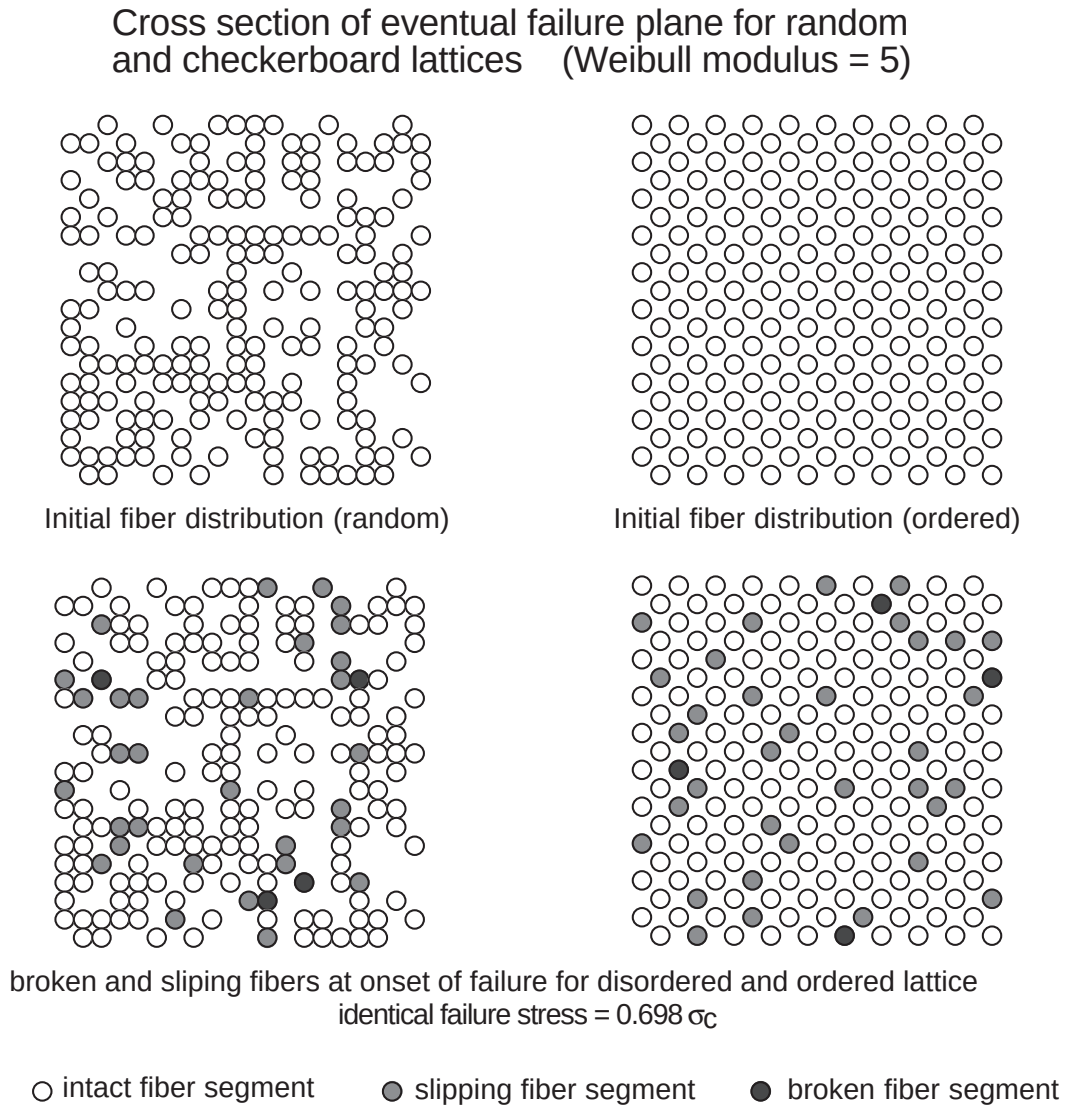

**Figure 3.11** Cross section of eventual plane of failure for both ordered (checkerboard) and disorded (random) lattices for Weibull modulus $m = 10$. At the failure stress of the disordered lattice, the ordered lattice has very sparse clusters of damage and more stress must be applied to "grow" these clusters into a size large enough to cause failure of the entire lattice.

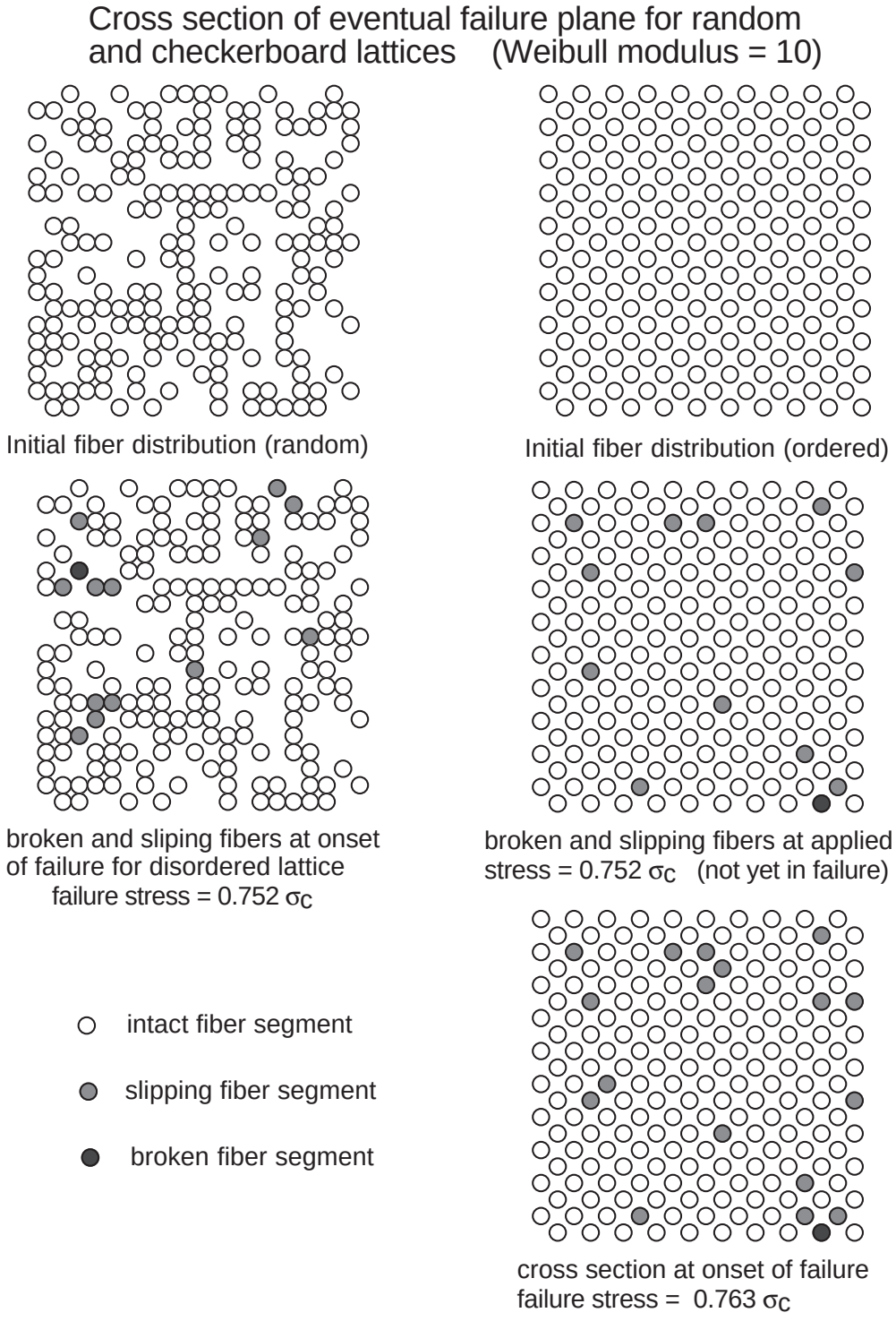

**Figure 3.12** Predicted scaling of strength with increasing composite size (number of fibers) for disordered lattice and corresponding ordered (checkerboard) lattice. Range shown corresponds to approximately 45 fibers ($n = e^{(1.95)^2}$) up to 14,900 fibers ($n = e^{(3.1)^2}$)

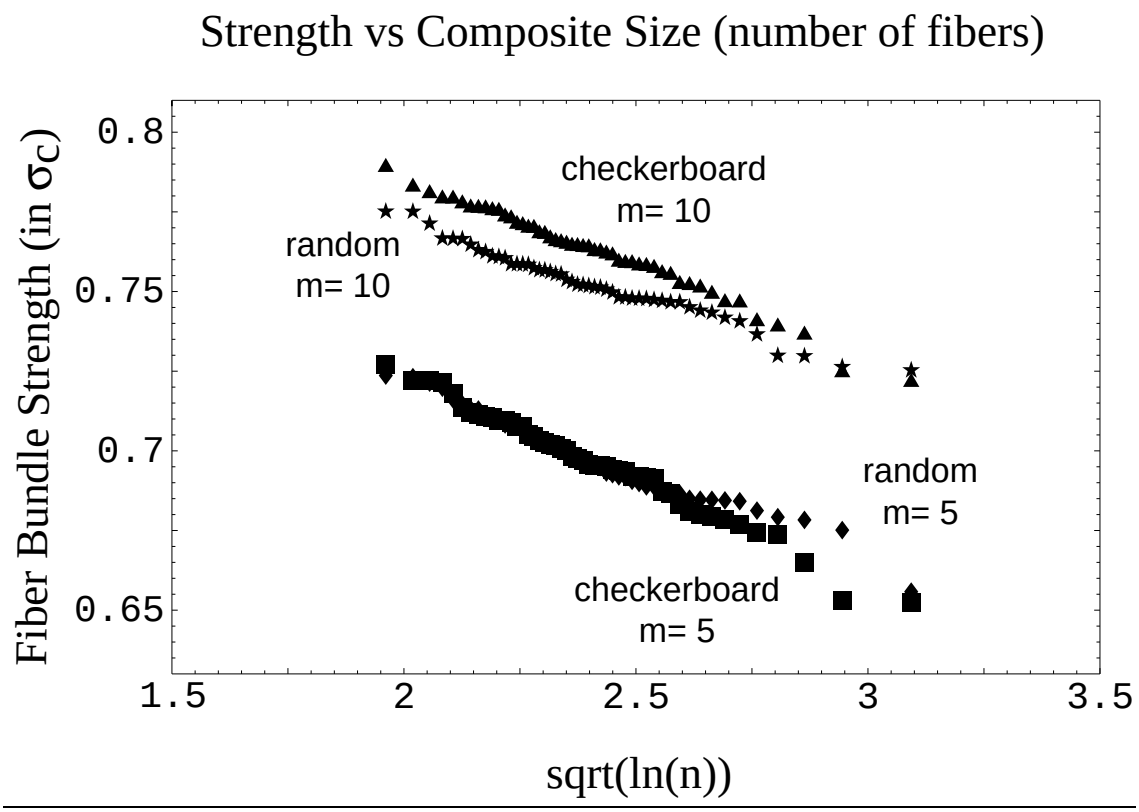

## 3.6 Load Gradients: Flexure Testing

In simple beam theory, the stresses in the direction of the width of the beam (the $z$-direction in Figure 3.13) can often be neglected for beams undergoing most types of simple bend loading. This is the case of plane stress, and for such a geometry we can assume $\sigma_z \simeq \tau_{xz} \simeq \tau_{yz} \simeq 0$, which accounts for three of the six components of the stress. Furthermore, stress analysis of bending geometry shows that $\sigma_x = 0$ as well. This leaves only the stress in the $y$-direction and the shear $\tau_{xy}$. We will assume failure due to shear is not an issue, and concern ourselves only with the $y$-direction stress and its resulting distribution. Of interest to us is that this remaining stress component is in the same direction as the stress due to a tensile or compressive load, in fact each fiber under such a load is going to be either in tension or compression.

For the case of 3-point bending, the resulting stress on a portion of the beam is strictly a function of the $x$-$y$ location. If we consider $\sigma^*$ to be the maximum tensile stress on the beam (this stress occurs on the bottom side of the beam directly below the center support), the resulting stress distribution is

$$\sigma_{3pt} = \sigma^* \left(1 - \left|\frac{2y}{L}\right|\right) \left(\frac{x}{d}\right) \tag{3.6}$$

where the origin is the center of the composite, $-L/2 \leq y \leq L/2$, and $-d \leq x \leq d$. Note that the plane $x = 0$ is the neutral axis with the beam undergoing compression above this plane and tension below this plane.

In the case of 4-point bending, as in Figure 3.14, we can confine our interest to the portion of the beam between the inner supports. Since this is the area of greatest stress, failure tends to occur in the inner span (in fact, failure outside of the span is often do to shear effects or a serious manufacturing flaw). The stress distribution between the inner supports is identical to the ideal case of pure bending, whose stress gradient is even further simplified in that there is no longer a $y$-component; stress depends only on distance from the neutral axis:

$$\sigma_{4pt} = \sigma^* \left(\frac{x}{d}\right) \tag{3.7}$$

When we apply these stress gradients to various models we will consider $\sigma^*$ to be the applied stress.

## 3.7 Modeling Flexure Load Gradients

In the tensile numerical LLS model, failure of a fiber segment is determined by comparing the segment strength with the sum of the transferred loads from broken/slipping fibers in the neighborhood and the applied load. This is easily modified

**Figure 3.13** Plane stress flexure (3-pt bend)

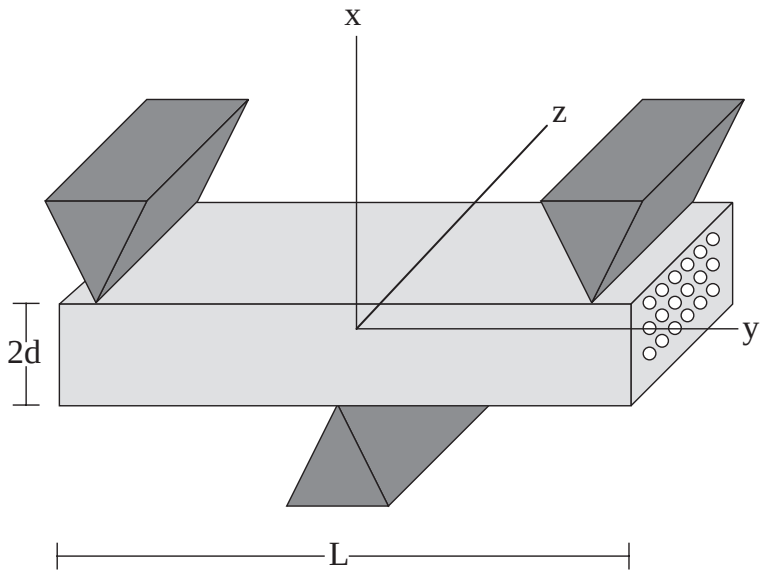


for the case of flexure by comparing the segment strength to the sum of transferred load and the local applied load, which is the global load modified by the stress distribution defined above.

For flexure problems, the stress distribution is purely a function of the location of a fiber segment in the sample, but this can easily be modified to include other variables.

Since, under flexure, the fibers are under compression (negative stress) on one side and under tension (positive stress) on the other, it is necessary to use the free-boundary implementation of the LLS model.

We assume that the fibers will not fail under compression. That is not to say that fibers below the center of the composite will not fail, but we will only consider tensile failure (redistributed tensile stress may overcome the compressive stress to break the fiber). In fact the effects of stress redistribution effectively and naturally moves the neutral axis as the composite fails.

To simplify (as well as speed up) the simulation, the failure criterion for bending is considered to be the formation of a *half-plane* of slipping or broken fibers below the center of the composite (rather than a plane that splits the composite). The assumption is that a stress sufficient to cause this plane to fail is sufficient to put the simulation into the regime of catastrophic failure (no additional stress needed to fail the composite, redistributed stresses are causing a cascade of failures). This also

**Figure 3.14** Beam under 4-point bend

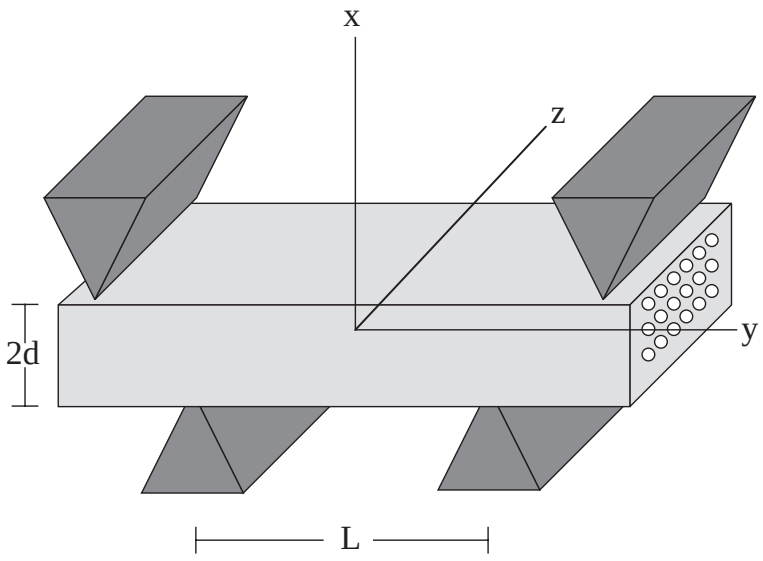


seems to be a reasonable assumption in that many physical specimens do not fail cleanly. Vindication of this criterion awaits comparison to experiment in Chapter 4.

## 3.8 A Modified Batdorf Model for Flexure

Here we attempt to generalize the Batdorf concept to include the effects of a non-uniform load distribution. If a composite under flexure has sufficiently many layers of fibers between the top and bottom supports, the difference in local stress gradient from one fiber to an adjacent fiber (above or below), is minimized. If we confine ourselves to the portion of the beam above the neutral axis, all fibers are under tension, with the tensile stress varying from zero at the neutral axis to it maximum at the top surface of the beam. Thus we are using our previous failure criterion: failure of the top half of the composite. Locally, a few layers would behave very much like they would in simple tension. We calculate the expected number of fiber failures in each layer using the local stress gradient, but then assume clusters grow as if nearby layers were undergoing identical stress. The key difference between this treatment and the previous tensile Batdorf model is that we look at failures and portions of failure clusters in each layer of the composite rather than the entire composite.

As in the previous treatment, all failures are assumed to occur in a single cross-

sectional plane, where we will now consider individual rows in this plane. The assumption that all failure occur in a single plane is actually very reasonable in the case of 3-point bending where the highest stress concentrations occur in the center of the beam. We assume the beam is $\mathcal{N}$ fibers in width and $\mathcal{M}$ in height. The length $L$ is taken to be the distance between the inner supports (4-point bending) or the outer supports (3-point bending) as in Figures 3.13 and 3.14.

The number of 1-plets in a single $j$ layer of $\mathcal{N}$ fibers undergoing 4-point bending is given by

$$Q_1^{(j)} = \frac{\mathcal{N}L}{\delta_c}\left(\frac{\sigma(x)}{\sigma_c}\right)^m \tag{3.8}$$

This quantity is slightly changed for 3-point bending since the probability of failure in a fiber segment varies with distance from the center support. The number of 1-plets in a single $j$ layer of $\mathcal{N}$ fibers undergoing 3-point bending is given by

$$Q_1^{(j)} = \frac{\mathcal{N}L}{\delta_c}\left(\frac{\sigma(x)}{\sigma_c}\right)^m \frac{1}{m+1} \tag{3.9}$$

We follow our previous development of the Batdorf model for tension with the difference that we are calculating the *portion* of a failure cluster residing in a layer $j$ and we have replaced the global applied stress $\sigma$ with the local layer stress $\sigma(x)$.

Solving the recursion relation (for 4-point bending) gives

$$Q_i^{(j)} = \frac{\mathcal{N}L}{\delta_c}\left(\frac{\sigma(y)}{\sigma_c}\right)^{i(m+1)-1} \prod_{j=1}^{i-1} \frac{n_j(c_j^{m+1}-1)}{(c_j-1)(m+1)} \tag{3.10}$$

The number of $i$-plets in the top half of the composite is given by

$$Q_i = \sum_{j=1}^{\mathcal{M}/2} Q_i^{(j)} \tag{3.11}$$

Combining this with $\sigma(x) = (2j/\mathcal{M})\sigma$ yields $Q_i$, the number of clusters of size $i$;

$$Q_i = \frac{\mathcal{N}L}{\delta_c}\left(\frac{\sigma}{\sigma_c}\right)^{i(m+1)-1} \left(\prod_{j=1}^{i-1} \frac{n_j(c_j^{m+1}-1)}{(c_j-1)(m+1)}\right) \sum_{j=1}^{\mathcal{M}/2} \left(\frac{2j}{\mathcal{M}}\right)^{i(m+1)-1} \tag{3.12}$$

At any stress $\sigma$, the above scheme generates a set of $\{Q_i\}$ values. The point of failure is then found as that stress at which there is a cluster size $i^*$ which simultaneously satisfies the conditions

$$Q_{i^*} = 1 \tag{3.13}$$

$$Q_{i^*+1} > Q_{i^*} \tag{3.14}$$

The first condition states that there is typically one cluster of size $i^*$ in the entire system. The second, critical, condition states that the $i^*$ system is actually unstable to growth to size $i^*+1$ at the current stress. Both conditions are necessary for failure to occur.

Here we have assumed that clusters grow and redistribute stress in the same manner as the tensile Batdorf model, and for simplicity we use the same values of near neighbors $n_i$ and concentration factors $c_i$, those of Hedgepeth and van Dyke (1967), as tabulated in Table 2.2. We have assumed that the composite is sufficiently large that these values are at least approximately valid. Clearly for small systems where the stress gradient changes substantially from layer to layer will result in cluster shapes and concentration factors significantly different from the tensile system.

## 3.9 Summary

We have extended the LLS simulation model to include the effects of free boundaries. Comparisons to a periodic boundary were done for a particular fiber geometry (corresponding to the coupons used by Gundel and Wawner (1997)) and found to have no statistical difference in strength at the composite length measured.

Using the methods that allowed for the creation of free boundaries in the LLS model, the effects of spatially disordered fiber arrangements were examined on lattices consisting of 200 fibers. The disordered lattices were found to have a strength distribution similar to the corresponding ordered lattice, but whose mean decreased with increased Weibull modulus. Size scaling methods were used to predict the strength of composites with sizes ranging from 45 to 14,900 fibers based on the 200 fiber lattice data.

Utilizing the free boundaries, the LLS simulation was again extended for the case of non-constant load gradients, specifically the load gradients undergone by specimens under flexure testing.

A Batdorf based model was developed for the modeling of thick composites under flexure.

# Chapter 4

# Comparison to Experiment

*On two occasions I have been asked [by members of Parliament], 'Pray, Mr. Babbage, if you put into the machine wrong figures, will the right answers come out?' I am not able rightly to apprehend the kind of confusion of ideas that could provoke such a question.*

—Charles Babbage

## 4.1 Tension

### 4.1.1 Ti-1100/SCS-6

Gundel and Wawner (1997) have recently presented a very detailed study of the properties of Ti-1100 matrix material reinforced with SCS-6 SiC fibers. Gundel and Wawner prepared panels of varying fiber volume fraction. They then painstakingly extracted fibers from as-processed coupons and performed single fiber tensile tests to determine the fiber strength distribution in each panel. The in-situ, or post-processed, fiber strengths showed some deviations from the pristine fiber strengths and, more importantly, showed substantial panel-to-panel variations that have a marked influence on the composite tensile strength. Most of the panels showed strength distributions following a Weibull distribution, and the characteristic strength $\sigma_o$ measured at a gauge length $L_o = 1$" and Weibull modulus $m$ for the different panels are shown in Table 4.1.

Gundel and Wawner also performed fiber pushout tests on individual fibers in each set of panels to obtain the interfacial sliding resistance $\tau$, shown in Table 4.1. Although the pushout test geometry and loading are not identical to the situation around an internal fiber break, pushout-derived sliding resistances follow the trends measured by other techniques and so we consider them fairly reliable. The sensitivity of the strength predictions to $\tau$ is also not too strong. The matrix yield stress was

**Table 4.1** Measured constitutive properties of Ti-1100 MMC (Samples B through I, fiber radius $r = 70\mu m$ at gauge length $L_o = 1$ inch) and Ti-6Al-4V MMC materials (Sample RZL, $r = 50\mu m$, $L_o = 1$ meter), and calculated values of the characteristic strength $\sigma_c$ and length $\delta_c$.

| **Sample** | $f$ | $m$ | $\sigma_{\mathbf{o}}$ (MPa) | $\tau$ (MPa) | $\sigma_{\mathbf{c}}$ (MPa) | $\delta_{\mathbf{c}}$ (mm) |
|---|---|---|---|---|---|---|
| B | 0.15 | 10.1 | 3930 | 188 | 5082 | 1.892 |
| C | 0.18 | 13.9 | 4310 | ≈190 | 5191 | 1.913 |
| D | 0.20 | 5.8 | 2890 | 190 | 4608 | 1.698 |
| F | 0.26 | 12.3 | 4270 | ≈65 | 4856 | 5.229 |
| G | 0.28 | 12.6 | 4640 | ≈65 | 5229 | 5.632 |
| H | 0.30 | 6.8 | 3330 | 65 | 4280 | 4.609 |
| I | 0.35 | 11.6 | 4410 | 81 | 5126 | 4.430 |
| RZL | 0.33 | 5.3 | 1470 | 140 | 4820 | 1.85 |

determined to be $\sigma_y = 935$ MPa. Finally, Gundel and Wawner performed tensile tests on coupons from each of these panels, using specimens containing essentially a fixed number of fibers and a gauge length of 1.5". The average strengths for coupons from each panel are shown in Table 4.2. Samples A and E of (Gundel and Wawner, 1997) are not shown in Tables 4.1 and 4.2 because these samples displayed a bimodal fiber strength distribution and so did not neatly fit into most analytic models. However, provided the relative populations of high and low strength fibers are available, the simulation model could be easily extended to handle multiple fiber strength distributions.

With the above detailed information on specific specimens, we have used the numerical LLS simulation model to predict the tensile strengths of each set of specimens. The inputs to the theory are the fiber strength distribution ($\sigma_o$, $m$ at $L_o$), interfacial sliding $\tau$, and fiber radius of $r = 70$ $\mu$m which are used to determine the normalizing parameters $\sigma_c$ and $\delta_c$ via Eqs. 2.2, shown in Table 4.1. We also use 104 fibers of length 1.5" in a thin strip geometry of 4x26 fibers, which closely approximates the dimensions of the specimens tested. We are thus essentially directly simulating the physical composites tested in the laboratory by Gundel and Wawner (1997). The output of the simulation model is a value for the bundle strength $\sigma_f^*$, which is then combined with the volume fraction $f$ and $\sigma_y$ in Eq. 1.13 to obtain the composite UTS.

Results of the simulated tensile strengths of the Gundel and Wawner (1997) composites are shown in Figure 4.1 and Table 4.2.

The agreement between measured and predicted strengths on specific samples

**Table 4.2** Composite tensile strengths (in MPa) for Ti-1100 MMCs and Ti-6Al-4V MMC as measured and as predicted by the LLS model (periodic and free-edge), GLS model, Rule-of-Mixtures, and Batdorf-type model. Also shown are the predicted average fiber pullout lengths as predicted by the LLS model.

| **Sample** | **Measured** | **LLS** (periodic) | **LLS** (free-edge) | **GLS** | **ROM** | **Batdorf** | **LLS pullout** ($\mu$m) |
|---|---|---|---|---|---|---|---|
| B | 1252 | 1341 | 1348 | 1392 | 1384 | 1334 | 210 |
| C | 1300 | 1470 | 1474 | 1531 | 1543 | 1464 | 220 |
| D | 1230 | 1353 | 1367 | 1414 | 1326 | 1319 | 190 |
| F | 1496 | 1630 | 1643 | 1708 | 1802 | 1631 | 600 |
| G | 1724 | 1768 | 1789 | 1856 | 1972 | 1766 | 650 |
| H | 1327 | 1535 | 1546 | 1605 | 1654 | 1502 | 550 |
| I | 1716 | 1929 | 1938 | 2041 | 2151 | 1900 | 510 |
| RZL | 1482 | 1572 | | 1674 | | 1442 | |

is excellent, typically being within 10%. The predicted values also follow some of the observed trends. For instance, Sample D has a strength comparable to Sample B in spite of a larger fiber fraction because of its anomalously low fiber strengths and Weibull modulus. For comparison, two other strength predictions are shown in Table 4.2 and Figure 4.1: the GLS value from Eq. 2.3; and the Rule-of-Mixtures (ROM) obtained by simply replacing $\sigma_f^*$ with the measured $\sigma_o$ in Eq. 1.13. The GLS value is always larger than the LLS value, and so agrees less well with the data; the differences between LLS and GLS are not too large here, however, because of the fairly small physical coupon size tested. The ROM strengths are generally even larger than the GLS predictions and are typically 100-200 MPa larger then the LLS predictions, and are also independent of composite size. The relative differences between models appear small in part because of the large contribution of the matrix to the composite strength in all cases. While all three models follow the general trends, the LLS model consistently narrows the difference between theory and experiment in all cases.

Interestingly, the influence of free-surface boundaries in a strip geometry is almost negligible. Results for the 4-fiber width system with periodic boundaries actually show slightly lower strengths (10-20 MPa) then for the free-surface 4-fiber width system. Thus, the higher stress concentration on fewer fibers that occurs in the free-edge geometry is slightly beneficial to the strength. Such results cannot be anticipated a priori. In fact our prior simulations (of shorter composites) in Chapter 3 suggested that differences in strength due to free-surface boundaries were not of statistical significance. From a design perspective, it is useful to know that the overall ply thickness does not have a detrimental effect on tensile strength

**Figure 4.1** Ultimate tensile strengths (in MPa) for samples studied by Gundel and Wawner (see Table 4.2 also), as measured experimentally and predicted by the Local Load Sharing, Global Load Sharing, Rule-of-Mixtures, and Batdorf-type models, respectively. All predictions generally follow trends in the experimental data, but the LLS and Batdorf models give the best agreement and differ from experiment by only 10% on average.

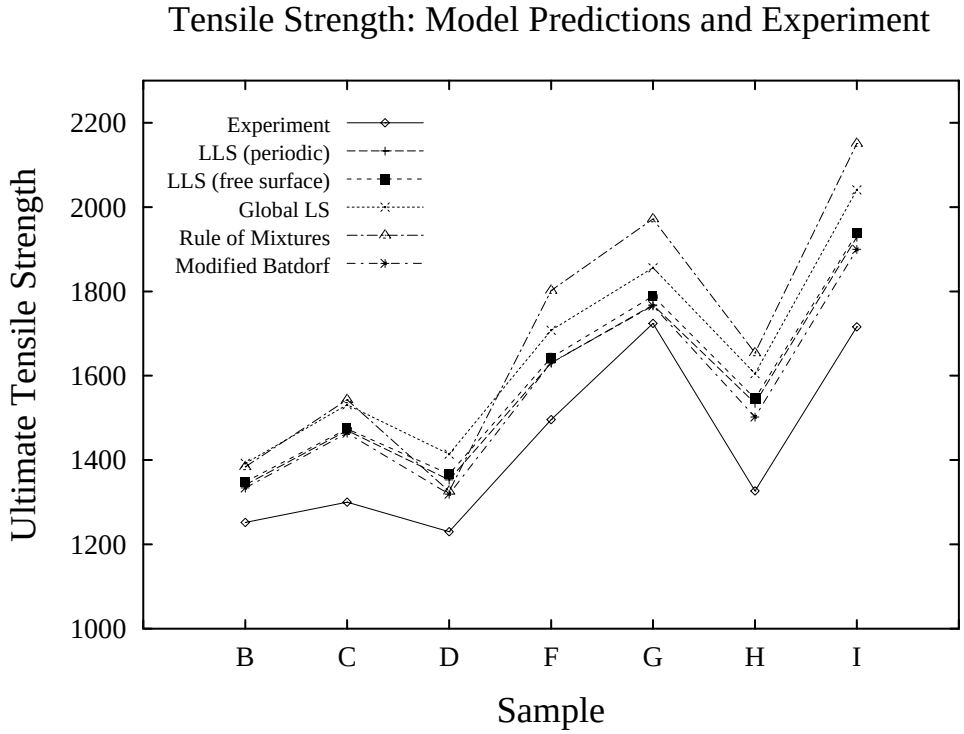


even for fairly thin specimens. The use of a square fiber array in the simulations, rather than a hexagonal array, might cause some differences between theory and experiment but those difference are probably not large, in light of the results found here using free-edge specimens.

At the end of the simulation, the plane of separation of the material can be determined and pullout length calculated. In GLS, the average pullout length is predicted to be $\langle L \rangle = \frac{1}{4}\lambda(m)\delta_c$ where $\lambda(m)$ depends slowly on $m$ and is around unity. In LLS, $\langle L \rangle$ is still controlled by $\delta_c$ but the coefficient $\lambda$ can differ, and is usually smaller. Taking the values of $\lambda(m)$ from Curtin (1991), the predicted pullout lengths, according to GLS, are $\approx 400$ $\mu$m for samples B,C,D (high $\tau$) and range from 960 $\mu$m to 1210 $\mu$m for samples F,G,H,I (smaller $\tau$). The predicted pullout lengths, according to the LLS simulation (periodic-edges), are $\approx 200$ $\mu$m for samples B,C,D

and range from 510 $\mu$m to 650 $\mu$m for samples F,G,H,I. All materials tested by Gundel and Wawner (1997) exhibited pullout on the order of 200 $\mu$m Thus there is a discrepancy here for the smaller-$\tau$ materials, suggesting fiber fracture is more localized to a plane then predicted. It is not clear whether this is a limitation of the model or due to dynamic effects in the real composites when they undergo rapid failure upon reaching the UTS.

With the input of the materials tested by Gundel and Wawner to obtain $\sigma_c$ and $\delta_c$, the predicted strengths are shown in Table 4.2 and Figure 4.1. Interestingly, the predicted strengths of all the models are generally extremely close to those found in the simulation model. As might be expected, the best results come from the LLS model and the Batdorf model. In fact, the Batdorf model results are generally very slightly closer to the measured values than the simulation model strengths. The apparent differences between Batdorf and LLS simulation results are somewhat minimized by the additional strengthening from the matrix itself, which contributes around 700 MPa to the strengths, and makes relative differences appear smaller.

In the two cases with low-$m$ fibers (Samples D and H) the Batdorf result is actually slightly lower than the simulation model. This stems from one important difference between the Batdorf and simulation models: the role of fiber pullout. As discussed in Section 2.6, the absence of pullout in the Batdorf model is believed to be responsible for the slightly lower strengths for the low-$m$ material. It is also conceptually inconsistent since the probability of fiber breakage was determined including the possibility of failure well away from the plane of the previous breaks. The Batdorf model does lead to slightly better agreement with experiment in these cases, but this is an artifact of the no-pullout approximation. The pullout observed on the fracture surfaces of the Ti-MMCs is smaller than predicted by the simulation model for the materials with lower $\tau$ values, but it is not sensitive to the precise $m$ value.

### 4.1.2 Ti-6Al-4V/BP-Sigma

Ramamurty et al. (1998) have performed a similar study on the properties of a Ti-6Al-4V alloy reinforced with unidirectionally oriented Sigma SiC fibers. The strength distibution of the fibers (extracted from the composite), interfacial sliding resistance $\tau$ (measured by fiber pushout), and fiber volume fraction (measured at the fracture surface) are also shown in Table 4.1. The fibers were of radius $r =$ 50 $\mu$m and the characteristic strength $\sigma_o$ was measured at a gauge length of $L_o =$ 1 meter. This long gauge length explains the sharp contrast in gauge strength $\sigma_o$ between this fiber and similar fibers studied by Gundel and Wawner (1997) (who used a gauge length of an inch). Ramamurty et al. (1998) determined the matrix yield stress of their composite to be $\sigma_y = 820$ MPa. They performed uniaxial tensile

tests on panels of width 6mm and length 75 mm consisting of 6 plies of fibers with a total thickness of 1 mm. Our corresponding simulation consists of 240 fibers in a 6x40 geometry of length 75 mm.

Ultimate tensile strength experimental results and the model predictions for the Ramamurty et al. (1998) composite are shown in Table 4.2. Pullout results were not available for the experimental composite. The Weibull modulus ($m = 5.3$) of this composite was even lower than that of the Gundel and Wawner composite. As a result, not only is the Batdorf prediction closer to the experimental value then the other models, but it actually underestimates it. The LLS model is consistent, predicting a strength less than 7% above the experimental result.

A subtle advantage to using Monte-Carlo type modeling is that it is more straightforward when used to make predictions of the distribution and variability of phenomenon. Ramamurty et al. (1998) performed 9 tensile tests resulting in a mean strength of 1482 MPa and a standard deviation of 14.2 MPa. The uncertainty in the standard deviation ($1/\sqrt{2(9-1)} = 25\%$) is 3.6 MPa. This variability compares quite favorably to the LLS simulation. 50 simulations were performed resulting in a mean strength of 1572 MPa and a standard deviation of $14.4 \pm 1.5$ MPa.

## 4.2 Summary of Tensile Results

The level of agreement between the experimental results and the LLS simulation predictions for both composites is relatively good, especially when compared to the GLS model or the common ROM calculation. The Batdorf model is similarly good, especially for the lower Weibull modulus samples.

Differences between the present theory and experiment might be traced to a variety of sources. First, the precise value for matrix yield stress is not well-established. Second, the pushout value for $\tau$ is approximate. Third, the load sharing used in the theory is that of Hedgepeth and Van Dyke, and does not consider issues specific to the Ti-MMC system. Fourth, initial fiber damage might exist in these materials. Fifth, dynamic fiber fracture and interface damage are not incorporated into the present model. Given the reasonable agreement between theory and experiment, however, these issues may not be significant.

In summary, the LLS simulation model provides accurate predictions of Ti-MMC coupon strengths when the fiber, matrix, and interface constitutive information is well-established. Gundel and Warner have also shown that these models also predict the non-linear stress-strain above matrix yielding quite well. These results for strength demonstrate that the LLS model can form the basis for the further development of detailed predictive models for notch strength, damage tolerance, and time-dependent degradation and durability in Ti-metal Matrix Composites.

## 4.3 Flexure

Ramamurty et al. (1998) performed 4-point bend tests, in addition to the tensile tests, on the Ti-6Al-4V MMC. The coupons used for flexure testing were identical to those used in bending and the constitutive properties are displayed in Table 4.1. The composite flexure strength is derived from the moment equation and is slightly modified from the tensile case. Under flexure, the transistion of the matrix material from an elastic to plastic state is not uniform. The region of plasticity moves from the surface inward as the applied couple increases, resulting in an increase in the matrix contribution to the total strength. Here we write the average nominal bend strength as

$$\bar{\sigma} = f\sigma_f + (1-f)\frac{3}{2}\sigma_y \tag{4.1}$$

where $\sigma_f$ is the fiber bundle strength and $\sigma_y$ is the matrix yield strength. The matrix yeild strength makes a large contribution to the overall bend strength, which can tend to mute differences due to differing fiber bundle strengths predicted by the various models. To compare the results of Ramamurty et al. (1998) with our model predictions we will derive the theoretical bundle strength of the experimental results from Equation 4.1. The 4-point bending was performed with an inner span length of $L = 9$mm (see Figure 3.14), and this is the length used for our various model predictions (the outer span was 27mm). Estimates and predictions of the fiber bundle strength of the Ti-6Al-4V MMC are tabulated in Table 4.3.

**Table 4.3** Fiber bundle strength estimates and predictions for the Ti-6Al-4V MMC under 4-point bending.

| **Predicted Fiber Bundle Strengths (in MPa)** | |
|---|---|
| Experimental estimate | 5180 |
| Estimate from strain measurement | 4980 |
| Local Load Sharing simulation | 5070 |
| Global Load Sharing (top layer) | 3050 |
| Batdorf Flexure | 2980 |

Ramamurty et al. (1998) arrived at an average nominal bend strength of $\bar{\sigma} = 2520$ MPa. Combined with the matrix yield strength of $\sigma_y = 820$ MPa and a fiber volume fraction $f = 0.33$, the fiber bundle strength was predicted to be $\sigma_f = 5180$ MPa. Ramamurty et al. (1998) made an alternative estimate, taken from their

strain measurements, of 4980 MPa which is very similar to the result derived from the average nominal bend strength.

By assuming that failure occurs when the top surface of the material fails, a Global Load Sharing prediction can be made using only the top layer under simple tension, and results in a predicted fiber bundle strength of 3050 MPa which is significantly less than the experimental results. This result is best understood in light of the behavior of the LLS simulations.

For the sake of completeness a Flexure Batdorf calculation was made giving the lowest result of all the models, a predicted bundle strength of 2980 MPa, lower even then the GLS prediction. The fundamental assumption of the Flexure Batdorf model was that the composite had to be extremely thick. Since the Ti-6Al-4V MMC is only 6 fibers deep, and the model only considers the top 3 layers, this assumption is violated. It is therefore not surprising that the results for this model are extremely poor.

Simulations using the LLS model were made with the failure criterion that an applied stress causing failure of the top half of the composite was sufficient to fail the rest of the composite. Currently the numerical code implementing the LLS algorithm does not implement the correct transfer of load from broken fibers in the region of the composite under compression.

It is unknown whether or not this is a sufficient failure criterion for all systems, but the excellent agreement with the experimental results suggest that it is a good criterion for this system. At the very least this failure criterion forms a lower bound on the applied stress using the LLS model. Observations of failure during a LLS simulation seem to indicate that a failure criterion using just the top layer is *not* sufficient, and hence the GLS result should be low; the composite is capable of sustaining much more damage. Figure 4.2 shows the cumulative fiber failures versus stress in a typical LLS simulation. This plot is entirely analogous to experiments where the acoustic emissions of the specimen are measured while under failure, each "pop" representing a fiber failure. Failure of the top layer of the composite occurs at approximately 0.89 $\sigma_c$ (approximately 200 fiber breaks), which while higher then the strength predicted by GLS ($\approx 0.62\ \sigma_c$), is still lower then the applied stress reached by allowing failure to continue to the middle of the composite. Typically this stress curve is flattening out as it approaches the failure criterion. In the curve shown the simulation ends during a cascade of fiber breaks, which may indeed represent catastophic failure of the material. 35 LLS simulations were run, and the mean fiber bundle strength was predicted to be 5070 MPa with standard deviation 140 MPa which compares very favorably to the experimental estimates, differing by only 2.2%. Figure 4.3 illustrates the evolution of damage in the simulation for the top layers of the composite. Note that even after "cracks" have crossed the top layer, that layer continues to absorb damage and carry considerable load.

**Figure 4.2** Plot of cumulative fiber failures vs. applied fiber bundle stress under 4-point bending in a LLS simulation.

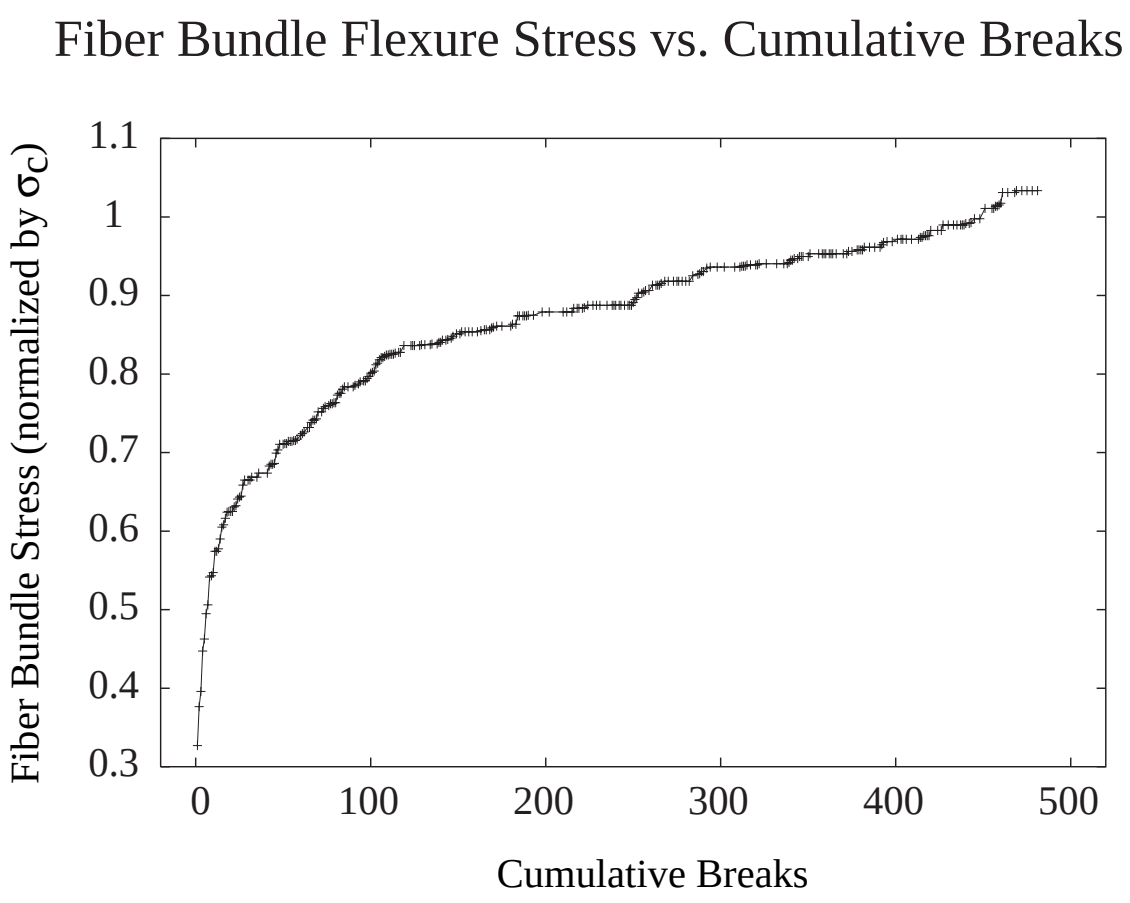

**Figure 4.3** Breaks in the top three layers of the simulated composite are shown for increasing 4-point bending stress. To simplify visualization, slipping regions around the fibers are not shown.

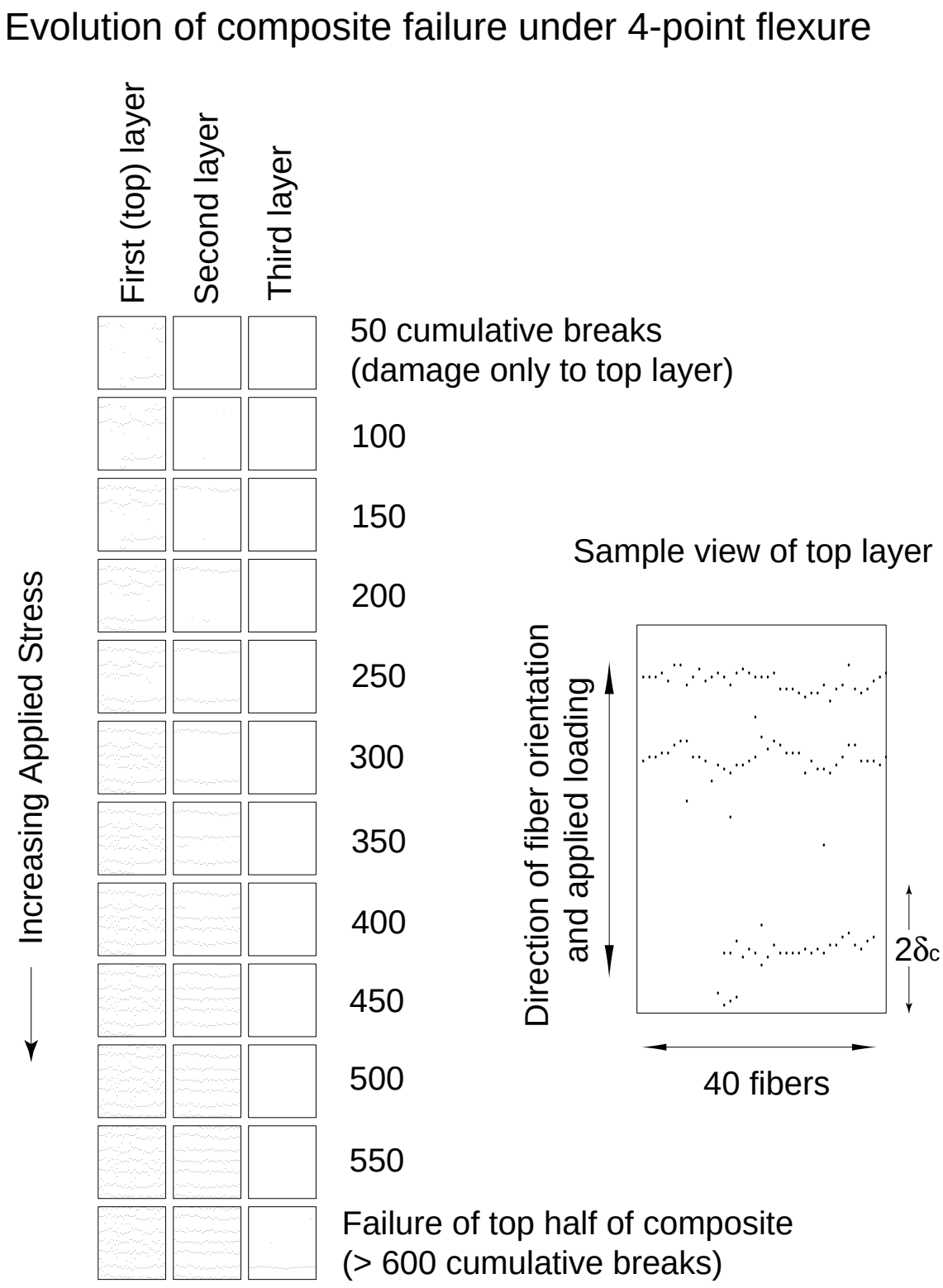

# Chapter 5

# Summary, Conclusions, and Future Work

*Work is the greatest thing in the world, so we should always save some of it for tomorrow.*

—Don Herald

We have applied a Local Load Sharing simulation model to predict the Ultimate Tensile Strengths of Ti-1100 and Ti-6Al-4V metal matrix composites. Furthermore we have extended the Local Load Sharing simulation model to predict the strengths of unidirectional fiber-reinforced composites under free-boundary conditions, non-constant load gradients, and arbitrary fiber spatial distribution. We have used these extensions to investigate the effects of disordered spatial fiber distributions on composite strength and applied an analytic model based on the Local Load Sharing simulations to predict the size scaling of strength in the disordered composites. We have used the extended Local Load Sharing model to predict the effects of flexure testing on a Ti-6Al-4V/Sigma SiC composite.

Utilizing measured constitutive properties, the Local Load Sharing model predicts tensile and flexure strengths in excellent agreement with the measured values with no adjustable parameters[1]. The model is thus predictive, given the as-processed fiber strengths for a particular material. The general model can then be used to assess the sensitivity of composite performance to variations in the constituent properties such as fiber strength and volume fraction, and interfacial sliding resistance. A modified tensile Batdorf model, which is an approximation to the LLS simulation model, shows equally good agreement with the measured results. However, the

[1]Since we picked the load sharing parameter $\Omega$ that corresponded to the stress concentrations derived by Hedgepeth and van Dyke (1967), rather than tuning it to experiment, we do not consider this an adjustable parameter.

predictions of the two models are rather different at lower Weibull moduli. The simulation-derived analytic model, which incorporates many sources of fluctuations which can influence strength, such as fiber pullout, appears to be more robust over a range of fiber Weibull moduli. A comparison of predicted notch strength also shows marked difference between the Batdorf-type and simulation-based models. A Batdorf-based model for the strength of thick composites under flexure was developed, but was found to be inappropriate in the modeling of the relatively thin measured coupons.

The LLS strength model, validated by the present detailed comparison to experiment, serves as a clear base for further modeling and understanding of MMC failure. Extensions to incorporate matrix creep behavior, time-dependent interfacial phenomena, and time-dependent fiber strength degradation, are all possible within the framework of the present model. The importance of composite size effects can also be understood within the present framework.

# Bibliography


Batdorf, S. B. (1982). Tensile strength of unidirectional reinforced composites – I., *Journal of Reinforced Plastics and Composites* **1**: 153–164.

Batdorf, S. B. and Ghaffarian, R. (1982). Tensile strength of unidirectional reinforced composites – II., *Journal of Reinforced Plastics and Composites* **1**: 165–176.

Beyerlein, I. J. and Phoenix, S. L. (1997). Stress concentrations around multiple fiber breaks in an elastic matrix with local yielding or debonding using quadratic influence superposition, *J Mech. Phys. Sol.* . in press.

Cox, B. N., Carter, W. C. and Fleck, N. A. (1994). A binary model of textile composites – I. formulation, *Acta Metallurgica et Materialia* **42**: 3463–3479.

Curtin, W. A. (1991). Theory of mechanical properites of ceramic–matrix composites, *Journal of the American Ceramic Society* **76**: 2837–2845.

Curtin, W. A. (1998). Size scaling of strength in fiber composites, *Physical Review Letters* **80**(7): 1445–1448.

Curtin, W. A. and Zhou, S. J. (1995). Influence of processing damage on performance of fiber-reinforced composites, *Journal of Mechanics and Physics of Solids* **43**: 343–363.

Du, Z.-Z. and McMeeking, R. M. (1995). Creep models for metal matrix composites with long brittle fibers, *Acta Metallurgica et Materialia* **43**: 701–726.

Fabeny, B. and Curtin, W. A. (1996). Damage-enhanced creep and rupture in fiber-reinforced composites, *Acta Materialia* **44**: 3439–3451.

Foster, G. C., Ibnabdeljalil, M. and Curtin, W. A. (1998). Tensile strength of fiber-reinforced composites: direct numerical simulation and analytic models, *International Journal of Solids and Structures* . in press.

Gundel, D. B. and Wawner, F. E. (1997). Experimental and theoretical assessment of the longitudinal tensile strength of unidirectional SiC fiber/titanium matrix composites, *Composites Science and Technology* **57**: 471–481.

Harlow, D. G. and Phoenix, S. L. (1981). Probability distributions for the strength of composite materials II: A convergent sequence of tight bounds, *International Journal of Fracture* **17**: 601–629.

Hedgepeth, J. M. and van Dyke, P. J. (1967). Local stress concentrations in imperfect filimentary composite materials, *Journal of Composite Materials* **1**: 294–309.

Hill, R. (1950). *The Mathematical Theory of Plasticity*, Oxford University Press, New York.

Hull, D. (1981). *An introduction to composite materials*, Cambridge University Press, Cambridge.

Ibnabdeljalil, M. and Curtin, W. A. (1997). Strength and reliability of notched fiber-reinforced composites, *Acta Materialia* **45**: 3641–3652.

Ibnabdeljalil, M. and Curtin, W. A. (1998). Strength and reliability of fiber-reinforced composites: localized load-sharing and associated size effects, *International Journal of Solids and Structures* **34**: 2649–2668.

Iyengar, N. and Curtin, W. A. (1997). Time-dependent failure in fiber-reinforced composites by fiber degradation, *Acta Materialia* **45**(4): 1489–1507.

Kachanov, L. M. (1971). *Foundations of the Theory of Plasticity*, North-Holland Publishing Company, Amsterdam.

Kelly, A. and Macmillan, N. H. (1986). *Strong Solids*, Clarendon Press, Oxford.

Knott, J. F. (1976). *Fundamentals of Fracture Mechanics*, John Wiley and Sons, New York.

MacKay, R. A., Draper, S. L., Ritter, A. M. and Siemers, P. A. (1991). A comparison of the mechanical properties and microstructures of intermetallic matrix composites fabricated by two different methods, *Metallurgical and Materials Transactions A* **25**: 1443–1455.

Phoenix, S. L., Ibnabdeljalil, M. and Hui, C.-Y. (1997). Size effects in the distribution for strength of brittle matrix composites: analysis and monte-carlo simulation, *International Journal of Solids and Structures* **34**: 545–568.

Piggott, M. R. (1980). *Load Bearing Fibre Composites*, Pergamon Press, Elmsford, New York.

Ramamurty, U., Zok, F. W. and Leckie, F. A. (1998). Assessment of the load transfer characteristics of a fiber-reinforced titanium composite.

Timoshenko, S. (1930a). *Strength of Materials: Advanced Theory and Problems*, D. Van Nostrand Company, Inc., New York.

Timoshenko, S. (1930b). *Strength of Materials: Elementary Theory and Problems*, D. Van Nostrand Company, Inc., New York.

Weber, C. H., Du, Z.-Z. and Zok, F. W. (1996). High temperature deformation and fracture of a fiber reinforced titanium matrix composite, *Acta Materialia* **44**: 683–695.

Weibull, W. (1939). The phenomenon of rupture in solds, *Proc. Ing. Vetenskapsakad*, number 153, Stockholm.

Weibull, W. (1951). A statistical distribution function of wide applicability, *Journal of Applied Mechanics* **18**: 293–297.

Whitney, J. M., Daniel, I. M. and Pipes, R. B. (1982). *Experimental Mechanics of Fiber Reinforced Composite Materials*, The Society For Experimental Stress Analysis, Brookfield Center, Connecticut.

Xu, J., Cox, B. N., McGlockton, M. A. and Carter, W. C. (1995). A binary model of textile composites – II. The elastic regime, *Acta Metallurgica et Materialia* **43**: 3511–3524.

Zhou, S. J. and Curtin, W. A. (1995). Failure of fiber composites: a lattice Green function model, *Acta Metallurgica et Materialia* **43**: 3093–3104.

# Notation

| | | | |
|---|---|---|---|
| $c_i$ | stress concentration factor | $\mathcal{M}$ | number of fibers in height direction |
| $f$ | fiber volume fraction | $\mathcal{N}$ | number of fibers in width direction |
| $l_s$ | fiber slip length | $\epsilon$ | composite strain |
| $m$ | Weibull modulus | $\bar{\delta}$ | discretization unit length |
| $n_c$ | critical bundle size | $\delta_c$ | characteristic length |
| $n_f$ | fiber bundle size | $\delta_l$ | length of a fiber bundle |
| $n_i$ | number of near neighbors | $\gamma^{**}$ | standard deviation of strength under GLS |
| $n_l$ | number of fibers in bundle | $\sigma$ | stress |
| $r$ | fiber radius | $\sigma_c$ | characteristic stress |
| $E_f$ | Young's modulus of fiber material | $\sigma_f^*$ | critical fiber bundle stress |
| $E_f$ | Young's modulus of matrix material | $\sigma_o$ | gauge stress |
| $H_n$ | fiber failure probability distribution | $\sigma_m$ | matrix stress |
| $L$ | composite/fiber length | $\sigma_u$ | ultimate tensile stress (composite failure) |
| $L_o$ | gauge length | $\sigma_y$ | matrix yield stress |
| $N$ | number of fibers in composite | $\tau$ | interfacial sliding resistance (shear) |
| $P_f$ | cumulative probability of fiber failure | $\mu^*$ | strength of bundle under GLS |
| $Q_i$ | number of $i$-plets | $\Omega$ | load sharing parameter |
| $Q_i^{(j)}$ | number of $i$-plets in layer $j$ | | |

# Abbreviations

| | |
|---|---|
| CMC | Ceramic Matrix Composite |
| GLS | Global Load Sharing |
| LLS | Local Load Sharing |
| MMC | Metal Matrix Composite |
| PMC | Polymer Matrix Composite |
| ROM | Rule Of Mixtures |
| UTS | Ultimate Tensile Strength |

# Vitæ

Glenn Craig Foster was born on March 16, 1969 to Dr. Beth Blodgett and Craig Foster in Sharon, Pennsylvania. After graduating from Tates Creek High School in Lexington, Kentucky, he enrolled in the University of Wisconsin at River Falls, becoming a member of the third generation of Fosters and Blodgetts to attend that esteemed institution. He completed his B.S. in Physics and Mathematics in May of 1992 and then spent the following year at Argonne National Laboratory as a student researcher.

In 1993 he entered Virginia Polytechnic Institute and State University and completed a M.S. degree in Mathematics approximately two and a half years later. Jumping to the Engineering Science and Mechanics department, Glenn plugged away for another few years and received another M.S., this one in Engineering Mechanics, in February 1998. In a futile attempt to hide from reality behind the walls of the ivory towers he has been working as an Instructor in the Virginia Tech Physics department as he steels himself for the jump to industry. In June of 1998 he will begin working for Siemens Energy and Automation, Inc. in Alpharetta, GA.